Title

Wireless Programmable Recording and Stimulation of Deep Brain Activity in Freely Moving Humans.

Journal

Neuron, 108(2)

ISSN

0896-6273

Authors

Topalovic, Uros
Aghajan, Zahra M
Villaroman, Diane
et al.

Publication Date

2020-10-01

DOI

10.1016/j.neuron.2020.08.021

Peer reviewed

HHS Public Access

Author manuscript

Neuron. Author manuscript; available in PMC 2021 October 28.

Published in final edited form as:

Neuron. 2020 October 28; 108(2): 322–334.e9. doi:10.1016/j.neuron.2020.08.021.

Wireless Programmable Recording and Stimulation of Deep Brain Activity in Freely Moving Humans

Uros Topalovic[1,2], **Zahra M. Aghajan**[2], **Diane Villaroman**[3], **Sonja Hiller**[2], **Leonardo Christov-Moore**[2], **Tyler J. Wishard**[2], **Matthias Stangl**[2], **Nicholas R. Hasulak**[4], **Cory S. Inman**[2], **Tony A. Fields**[5], **Vikram R. Rao**[6], **Dawn Eliashiv**[5], **Itzhak Fried**[2,3,7], **Nanthia Suthana**[2,3,8,9,10,*]

[1]Department of Electrical and Computer Engineering, University of California, Los Angeles, Los Angeles, CA 90095, USA

[2]Department of Psychiatry and Biobehavioral Sciences, Jane and Terry Semel Institute for Neuroscience and Human Behavior, University of California, Los Angeles, Los Angeles, CA 90024, USA

[3]Department of Neurosurgery, David Geffen School of Medicine, University of California, Los Angeles, Los Angeles, CA 90095, USA

[4]NeuroPace, Mountain View, CA 94043, USA

[5]Department of Neurology, University of California, Los Angeles, Los Angeles, CA 90095, USA

[6]Department of Neurology and Weill Institute for Neurosciences, University of California, San Francisco, San Francisco, CA 94143, USA

[7]Tel Aviv Sourasky Medical Center and Sackler Faculty School of Medicine, Tel Aviv University, Tel Aviv 69978, Israel

[8]Department of Bioengineering, University of California, Los Angeles, Los Angeles, CA 90095, USA

[9]Department of Psychology, University of California, Los Angeles, Los Angeles, CA 90095, USA

[10]Lead Contact

SUMMARY

Uncovering the neural mechanisms underlying human natural ambulatory behavior is a major challenge for neuroscience. Current commercially available implantable devices that allow for recording and stimulation of deep brain activity in humans can provide invaluable intrinsic brain

*Correspondence: nsuthana@mednet.ucla.edu.

AUTHOR CONTRIBUTIONS

Conceptualization, N.S., Z.M.A, and U.T.; Methodology and Software, U.T., Z.M.A., D.V., S.H., N.R.H, and T.A.F.; Investigation, U.T., Z.M.A., D.V., S.H., L.C-M, T.J.W., M.S., C.S.I., and D.E.; Resources: N.R.H., I.F., V.R.R. and N.S.; Writing–Original Draft, U.T. and N.S; Writing–Review and Editing, U.T., N.S., Z.M.A., M.S., C.S.I., and N.R.H; Visualization, U.T.; Funding, N.S.

DECLARATION OF INTERESTS

N. R. H. is an employee of NeuroPace, Inc., Mountain View.

signals, but are not inherently designed for research and thus lack flexible control and integration with wearable sensors. We developed a mobile deep brain recording and stimulation (Mo-DBRS) platform that enables wireless and programmable intracranial electroencephalographic recording and electrical stimulation integrated and synchronized with virtual/augmented reality (VR/AR) and wearables capable of external measurements (e.g., motion capture, heart rate, skin conductance, respiration, eye-tracking, and scalp EEG). When used in freely moving humans with implanted neural devices, this platform is adaptable to ecologically valid environments conducive to elucidating the neural mechanisms underlying naturalistic behaviors and to the development of viable therapies for neurologic and psychiatric disorders.

Keywords

Neuroimaging Methods; Human; Intracranial EEG; Intracranial Electrical Stimulation; Wearables; Virtual Reality; Augmented Reality

INTRODUCTION

Traditional methods for recording and modulating brain activity in humans (e.g., fMRI, MEG, TMS) require immobility and are thus limited in their application during laboratory-based tasks low in ecological validity. Given the recent increase in medical therapies using implanted neural devices to treat and evaluate abnormal brain activity in patients with epilepsy (Schulze-Bonhage et al., 2017) and other neurologic and psychiatric disorders (Benabid et al., 1987; Vidailhet et al., 2005; Ressler and Mayberg, 2007; Nuttin et al., 1999; Lozano et al., 2016), recording and modulating deep brain activity during freely moving behavior is now possible. There are currently over two thousand individuals with chronic sensing and stimulation devices implanted within the brain, with the number expected to increase as additional invasive treatments are proven successful. The range of brain areas available for study in these participants is diverse since electrodes are placed within a variety of cortical (e.g., orbitofrontal, motor, temporal cortices) and subcortical (e.g., medial temporal lobe, basal ganglia) areas depending on an individual's clinical diagnosis. The benefits of a mobile deep brain recording and stimulation platform are invaluable, for example, in studying behaviors that can provide theoretical links with animal neurobiology and systems neuroscience that are almost exclusively mobile (e.g., spatial navigation, social interaction). Clinical Neuroscience studies can also benefit from a mobile platform, for example, to test novel responsive neurostimulation therapies during naturalistic behaviors (e.g., walking, eating, socializing) in patients with implanted electrodes who suffer from neurologic and/or psychiatric disorders. Patient populations with implanted neural devices thus provide a rare scientific opportunity to directly record from and stimulate a variety of locations within the human brain during freely moving and clinically relevant behaviors without the confounds of immobility and motion-related artifacts present in other recording methods (Zaitsev, Maclaren, and Herbst, 2015; Parvizi and Kastner, 2018).

A few neuroscientists have begun to capitalize on the opportunity to use chronically implanted neural devices, such as the RNS® System (NeuroPace, Inc., Mountain View) (Aghajan et al., 2017; Meisenhelter et al., 2019; Henin et al., 2019; Rao et al., 2017).

However, these studies did not provide methods for real-time viewing and control nor the ability to deliver intracranial electrical stimulation (iES) and perform precise synchronization of intracranial electroencephalographic (iEEG) with externally acquired data during free movement. Other implantable systems have emerged such as the Medtronic Summit RC+S (Stanslaski et al., 2018; Kremen et al., 2018), an investigational device, intended for clinical research that allows for iEEG recordings and closed-loop iES, however, requires added externalized tools to enable its use for research studies.

Researchers have long recognized the necessity of unconstrained studies (Ladouce et al., 2017) even before implantable neural systems were available, which has led to increased utilization of wearable technologies (Lau-Zhu, Lau, and McLoughlin, 2019). A set of useful behavioral control measurements have been established, however, are often used separately and in an ad hoc fashion during stationary experiments since multivariate and synchronized mobile implementation is a challenge.

To address these challenges, we developed a first-of-its-kind mobile deep brain recording and stimulation (Mo-DBRS) research platform that enables systematic and wireless control over chronically implanted neural devices and synchronization with wearables that can record heart rate, respiration, skin conductance, scalp EEG, full-body movement/positional information, and eye movements. Mo-DBRS uses a combination of embedded electronics and software scripts added to the existing research-oriented, tethered RNS System used in previous studies (Meisenhelter et al., 2019) to enable remote, simultaneous, stable output from different wearable sensors along with their synchronization. The Mo-DBRS platform is primarily built and validated for the RNS System, given its relative wide-spread use (>2000 implanted), however, components can be integrated with other implantable systems (e.g., RC +S). When used in conjunction with virtual/augmented reality (VR/AR) technologies, the Mo-DBRS platform provides an ecologically valid environment to simulate real-world experiences and open a new area of research in the fields of basic, cognitive, and clinical neurosciences.

RESULTS

Mobile deep brain recording and stimulation

We implemented, characterized, and validated the Mo-DBRS platform in five research participants (Table S1) previously implanted with the RNS System (Figure 1A) with electrodes in a variety of medial temporal and frontal regions (Figure 1B, Tables S1, S2) for treatment of medically-refractory focal epilepsy in accordance with the product labeling. We also include example data from the Mo-DBRS platform used in two additional participants (seven total participants) implanted with the RNS Neurostimulator (see Mo-DBRS example data section). All participants volunteered for the study by providing informed consent according to a UCLA Medical Institutional Review Board (IRB) approved protocol. A central part of the platform is a set of externalized Research Tools, which allow for wireless and programmable control of the RNS System. The Tools can be carried by backpack in a Mo-DBRS Full (weight = ~9 lbs, Figure 1D) or Mo-DBRS Lite (weight = ~1 lb, Figure S1) wearable solution for use during ambulatory or stationary research studies.

Mo-DBRS Full

The full wearable version of the platform (Mo-DBRS Full, Figures 1C,D) provides real-time viewing, storage, and synchronization of iEEG data with external data, and on-demand triggering of iES. These functionalities can be accessible on an encrypted local wireless network through a TCP-based server running on a small board computer, Raspberry Pi (RP). The implanted RNS Neurostimulator communicates via Near Field Telemetry to a Wand (Figure 1D) placed on the participant's head, above the underlying implanted device (Figure 1C). A tablet or a laptop device (Programmer), to which the Wand is connected, contains a user interface that allows for manual control and data storage (Figure 1D). The Programmer, when used with a custom-built Programmer Tool (Figure 1D), accepts commands for iEEG storage (*Store* command) and iES delivery (*Stim* command). Commands for changing iES parameters are also available on the wireless server and should be sent separately before the *Stim* command. Parameters for iES are identical to those available on the commercially-available and FDA approved system: Current (0–12 mA; increments 0.5 mA / 0.1 mA for RNS-300M / RNS-320), Frequency (1–333 Hz), Pulse Width (40–1000 μs; increments 40 μs), Duration (10–5000 ms).

When used with an attached custom-built Wand Tool (Figure 1D), the Wand allows for the injection of a marking signal (via a *Mark* command) into the Real-Time iEEG data that can be used for synchronization. The Wand Tool can also deliver an electromagnetic pulse (via a *Magnet* command), which triggers the local storage of iEEG data on the RNS Neurostimulator. While iEEG data can be transferred to the Programmer in real-time and stored via the *Store* command, the *Magnet* command triggers the iEEG data to be saved on the RNS Neurostimulator, which can be retrieved later via the Wand. For remote programmable control of the RNS System, the RP decrypts incoming commands and forwards them to the Programmer Tool, and then to the Programmer (*Store* and *Stim*) or Wand Tool (*Mark* and *Magnet*) for final execution. The *Mark* and *Magnet* commands leave specific artifacts in the Real-Time iEEG data (*Mark*–Figure 2A, *Magnet*–Figure 2B, *Stim*–Figure 2C), which can be used for synchronization. Lastly, a custom-built Telemetry Switch can be used to disable on-demand telemetry ("kill switch") to prevent associated artifacts in scalp EEG data, and can be controlled by the RP (see STAR Methods). Research Tools in blue boxes (Figure 1D) are unique to the Mo-DBRS platform and have not been used in previous studies.

We validated the Mo-DBRS platform in two ways: 1) Ex-vivo (benchside) testing and characterization of wireless command latencies using an externalized test RNS Neurostimulator device, and 2) In-vivo testing and characterization of wireless command latencies in five (out of seven) participants implanted with the RNS Neurostimulator. Ex-vivo validation included measurements of 1) absolute latencies between command (*Store, Mark, Stim, Magnet*) initiation and completed delivery, and 2) relative latencies between the delivered commands (*Store*, *Mark*, and *Magnet*) and the recorded iEEG at command initiation. Absolute latencies describe the delay between command initiation and completion, while relative latencies describe the delay between command initiation and the onset of implementation reflected in the iEEG data. Although absolute and relative latencies depend on each other, for practical research purposes, the relative latencies are more

informative for synchronization with the Experimental Task Paradigm. When assessing the absolute and relative latencies of each command, the standard deviation (s.d.) compared to the mean is a more useful metric given that differences in mean values across data streams can be accounted for during synchronization. Relative latencies were measured because of the added latency associated with each sample of iEEG that travels from the analog front-end of the RNS System through digitization and telemetry before it is stored in the Programmer (Figure S2A). We did not measure relative latencies for the *Stim* command since iES is delivered and recorded at the electrode site and thus absolute and relative latencies are equal. Absolute latencies for all commands were assessed using an oscilloscope (see STAR Methods, Ex-vivo testing section for details).

Absolute command latencies were quantified during wireless and stationary (tethered, without the RP) setups using the Tablet and Laptop Programmer separately (Figure 2F). In the wireless setup, additional delays were introduced by the RP (latency: 2380 ± 142 μs; 1000 trials) and network transmission (latency: 149 ± 14 μs; 1000 trials). Overall, latencies were lower when using the Tablet compared to the Laptop Programmer, due to a more responsive interface and faster serial communication in the Tablet compared to the Laptop Programmer (57600 vs. 9600 bps). Commands that involve interactions with the Programmer (*Store* and *Stim*) had higher absolute latencies (*Store*: 1145.23 ± 35.87 ms and *Stim*: 1355.51 ± 26.4 ms for the Wireless Tablet setup, see Figure 2F for Tethered and Wireless Laptop setups) due to the lag introduced by the (Laptop and Tablet) Programmer's Graphical User Interface (GUI).

Relative latencies were measured by using the RP to send a command (*Store, Mark, Stim, or Magnet*) to the Programmer Tool and a simultaneous Reference Pulse (offset at the source = 22.5 ± 41.17 μs;) to a test RNS Neurostimulator electrode contact (Figure S2A, STAR Methods) to measure relative distance in time (Figures 2D,E). We found that *Marks* consistently appeared in the Real-Time iEEG 3–4 samples (mean ± s.d. = 13.78 ± 2.04 ms, Range = [12,16]; Figures 2D,E) before the Reference Pulse. The *Store* command relative latency was measured to be 282.27 ± 6.68 ms (Figure S2D). It should be noted that when using the Tablet Programmer the *Store* command is not needed since iEEG data is saved automatically in parallel to the ongoing Real-Time iEEG. Thus, there is no need to stop Real-Time iEEG transmission in order to store the iEEG data unless there is a need to partition chunks of saved iEEG data manually. Relative latencies for the *Stim* command are equivalent to absolute latencies (1355.51 ± 26.4 ms for the Wireless Tablet setup, Figure 2F). See the Mo-DBRS Lite section for *Magnet* command latencies.

In-vivo validation showed that execution of the *Store* and *Stim* commands required a minimum amount of time to pass between subsequent commands, during which Real-Time iEEG transmission stops and starts again once command implementation has been completed, thereby increasing the absolute latencies (Laptop Programmer: *Store*=4.6 s, *Stim*=2 s; Tablet Programmer: *Store*=2 s, *Stim*=1.5 s). These values were obtained by sending multiple consecutive commands and gradually lowering the step between them (e.g., *Stim* in Figure 2C). We also measured, in-vivo, the variability in delivery of *Mark/Magnet* commands and confirmed that the relative latency uncertainty (s.d.) was consistent with results from ex-vivo experiments (*Mark*: ~2.5 ms and *Magnet*: ~6.4 ms). During

Experimental Task Paradigms, Real-Time iEEG was viewed remotely from the Programmer, via screen-sharing programs over the network (Figures S3B,C,D) to confirm delivery of *Marks* and continuous telemetry (no iEEG dropouts). For more details see STAR Methods.

Mo-DBRS Lite

The lightweight version of the platform (Mo-DBRS Lite, Figure S1) uses an electromagnet device to trigger the RNS Neurostimulator's onboard storage via the *Magnet* command (Figure S1A), resulting in a record-only solution. Mo-DBRS Lite thus requires a separate stand-alone electromagnet device with sufficient driving power that can send a *Magnet* command, which can be triggered 1) with a physical button press, 2) repeatedly, every pre-configured number of seconds (Figure S1B), or 3) on-demand (Figure S1C) via a wireless network and an RP. For all three options, a visible LED worn externally (Figures S1B–D) and triggered simultaneously with the *Magnet* can be used to synchronize stored iEEG activity offline with externally acquired data from wearables. For the 3rd option, RP timestamp logs can be used in addition to the *Magnet* command and LED for synchronization purposes.

In general, synchronization is more accurate with Mo-DBRS Full compared to Mo-DBRS Lite. Mo-DBRS Full uses the *Mark* command and Real-Time iEEG whereas Mo-DBRS Lite stores iEEG data using the *Magnet* command, and hence, synchronization depends on the extracted *Magnet* timestamp. A *Magnet* event, once detected in the RNS Neurostimulator, triggers the storage of a predefined time period (fixed within the commercially available RNS System) such that 2/3 (1/3) of the data saved is before (after) the *Magnet* event. The detection of a *Magnet* is effectively sampled by the RNS Neurostimulator with a 2 Hz frequency, and thus a variable offset between the *Magnet*-triggered and consequently stored iEEG data occurs. To investigate further, we sent a series of *Marks* and Reference Pulse pairs followed by a *Store* and *Magnet* command in 20 repeated trials (Figure S2B) ex-vivo. Results showed that although the *Magnet* absolute latency was 11.24 ± 5.52 ms, the relative latency with respect to the iEEG storage point was 423.87 ± 78.99 ms (Figure S2E). Accuracy results are shown in Figures S2C–E. All absolute and relative latency results from Mo-DBRS Lite ex-vivo testing regarding *Magnet* delivery also apply to Mo-DBRS Full.

Mo-DBRS integration with other wearables

A unique aspect of the Mo-DBRS platform is that it can be used with participants wearing on-body sensors (wearables). The platform provides solutions for synchronization of iEEG, iES, and wearables (Figure 3) including full-body motion capture (Figure 3B), eye-tracking (Figure 3C), biometrics (heart rate, skin conductance, respiration, Figure 3D), and scalp EEG (Figure 3F). In addition to traditional 2-D computer-based tasks and real-world scenarios, the Mo-DBRS platform allows participants to view synchronized stimuli on VR/AR headsets (Figures 3A,H) that simulate real-world experiences under experimental control, while allowing for full head and body movements.

All wearable equipment can be connected to the same local network, and synchronized with the Experimental Task Paradigm using software timestamping, *Mark* commands, and other task-dependent visual/audio events captured by the wearables. Total uncertainty (s.d.) of the

relative latency of synchronization between iEEG and wearable data is ~16 ms (Mo-DBRS Full) and ~83 ms (Mo-DBRS Lite). Mo-DBRS Full relative latency uncertainty is further increased compared to Task-iEEG only (16 ms compared to 2 ms, Table 1) because of sampling frequency limitations related to wearables (e.g. motion capture cameras: 60 frames per second). The Mo-DBRS Lite relative latency uncertainty (s.d.) is unchanged, however manual triggering of the electromagnet increases this uncertainty from 78.99 ms (Figure S2E) to 83 ms (Table 2) related to an added delay associated with LED-based synchronization of iEEG with the Experimental Task Paradigm. An example participant wearing the Mo-DBRS Full platform is shown in Figure 3, with the underlying high-level code structure in Figure S3A. Experimental Task Paradigms seldom require all of the outlined components simultaneously and, therefore, the platform can be customized for a specific research study.

Researchers use a variety of stimulus presentation software programs on an Experimental Computer (Figure 3G) to implement Experimental Task Paradigms whether stationary or mobile. To expand usability, the Mo-DBRS platform includes open-source code solutions for the most commonly used programming environments (i.e., MATLAB, Unity, and Python), allowing researchers to adapt and upgrade their Experimental Task Paradigms to work with the Mo-DBRS platform (Figure S3A). We also provide a GUI solution for use on a phone/tablet (Figures S3B,C) for manual non-automated Experimental Task Paradigms.

Mo-DBRS integration with scalp EEG

While iEEG allows for recording of activity within specific deep brain structures, scalp EEG remains a prominent method to probe the human brain, as it is a more readily available methodology due to its non-invasive nature (Parvizi and Kastner, 2018; Ramantani, Maillard, and Koessler, 2016). The Mo-DBRS platform allows for simultaneous iEEG and scalp EEG (Figures 4, S4, S5)—an opportunity that can elucidate links between deep and surface brain activity and bridge findings across studies. To enable simultaneous iEEG and scalp EEG, we developed two solutions for minimizing the RNS System's telemetry-related artifacts in scalp EEG data, which are a result of the Wand's telemetry given that the scalp EEG cap is placed in between the Wand and the implanted RNS System. The 1st solution is a programmable switch for disabling/enabling telemetry (Telemetry Switch, Figures 4A, S4D–H), which disables RNS System telemetry when it is not necessary and utilizes the Mo-DBRS Full *Magnet* command to retrieve non-transmitted iEEG data (See STAR Methods and Supplementary Information). The 2nd method builds upon previous work (O'Shea and Shenoy, 2018; Islam, Rastegarnia, and Yang, 2016) for reducing stimulation and artifacts, by relying on Principal Component Analysis and Wavelet Transform (Figures 4, S5). These signal processing techniques were modified to correlate observed scalp EEG signal with the RNS System telemetry-specific templates and to filter out telemetry frequency bands in the time-frequency domain, resulting in 86.2% reduction of unwanted signal artifacts (Figures 4A,B), as reflected in the root mean square values (RMS) of the scalp EEG signals (Figure 4C).

Mo-DBRS example data

Example data recorded from a participant wearing the Mo-DBRS platform during which they were instructed to navigate to a wall-mounted sign in a 20 × 17.8 ft^2 room is shown in Figure 5 and Video S1. Two coordinate systems are shown, one relative to the room (Motion Capture; Figure 5B) and the other relative to the participant's head (Eye-tracking; Figure 5C). Example iEEG data from additional participants is shown in Figure S6 and data from other wearables in Figure S7.

Quality of iEEG data depends on the physical stability of the Wand placement on the participant's head, which can cause data loss (Figure S6E) temporarily if unstable. Only 1 participant (out of 7 total) experienced iEEG data loss where 2.3% of total data was discarded due to dropouts. Lastly, epileptiform activity (Figure S6F) was detected (1.27% on average across participants) using previous methods (see the Removing epileptiform activity section in STAR Methods). No artifacts due to VR/AR headsets were present in iEEG and scalp EEG data, expectedly since VR/AR electronics and communications operate at much higher frequencies (MHz or GHz) compared to iEEG (250 Hz) and scalp EEG (2000 Hz).

DISCUSSION

Currently, in the fields of Cognitive and Clinical Neuroscience, naturalistic behavioral paradigms with rich behavioral data limit the recording of human neural data, while paradigms comparatively rich in neural data are almost impossible to carry out in naturalistic settings. The Mo-DBRS platform provides a new method for modulating and interrogating the human brain during naturalistic behaviors with ecologically valid tasks. It enables wireless and programmable iEEG and iES synchronized with biological and behavioral data via wearable technologies. We provide the functionalities and details necessary for building and optimizing the Mo-DBRS platform—during ambulatory (Figure 6A) or stationary (Figure 6B) behavioral paradigms—through real-time wireless control of sensing, stimulation, and synchronization with external devices such as eye-tracking/VR/AR headsets (Figures 6A,D) and other behavioral measurements (Figure 6C). Several components of the platform, including open-source code for wireless programmable synchronization with wearables, can be adapted for use with other existing implantable neurostimulation devices (e.g., Medtronic Summit RC+S) or those in development. In addition, when used in patients with neurologic and psychiatric disorders along with continuous behavioral metrics, the Mo-DBRS platform provides an opportunity to characterize neural mechanisms and develop and test novel treatments.

Comparison with previous reports

The Mo-DBRS platform includes three key improvements compared to previous work (Aghajan et al., 2017; Meisenhelter et al., 2019; Henin et al., 2019; Rao et al., 2017): 1) improved accuracy of synchronization, 2) mobility, and 3) integration with multiple wearables. Importantly, the *Mark*-based synchronization method (Meisenhelter et al., 2019) has an improved relative latency (14 ± 2 ms), and can be used during freely moving behaviors. Mo-DBRS Lite provides a programmable and remote solution for *Magnet*-based synchronization methods used previously (Aghajan et al., 2017). We also report the

uncertainty of *Mark* and *Magnet* command relative latencies with respect to actual recording channels and thereby consider *Mark* and *Magnet* artifact shifts in the iEEG data, unlike in previous studies (Aghajan et al., 2017; Meisenhelter et al., 2019) (Table 1). The Mo-DBRS *Mark*-based synchronization solution is also more reliable than camera-based solutions (that record the Programmer's screen, task-related events, and/or known neural responses in iEEG) used in previous studies (Rao et al., 2017) and is thus not limited by associated uncertainties (e.g. responsiveness of the Programmer's GUI or variability of neural responses across participants). Further, Mo-DBRS Full allows for continuous recordings without the need for restarting of synchronization methods if telemetry is lost and/or after breaks between experimental sessions. Altogether, Mo-DBRS provides a single, flexible framework with multiple neural and behavioral measurements that can be used in ambulatory tasks with hardware and software details included to enable others to build the platform in their own laboratories.

Trade-offs and Limitations

While there are clear advantages in adopting the Mo-DBRS platform to provide a unique window into the human brain during naturalistic behaviors, future studies should be cognizant of limitations related to iEEG recordings in patients with neurologic or psychiatric disorders (Parvizi and Kastner, 2018). Also, it should be borne in mind that the specific wearable platform version (i.e., Mo-DBRS Full or Lite) affects the system setup and thus, the trade-offs between the wearability and capabilities should be considered during the Experimental Task Paradigm design (Table 2).

Mo-DBRS Full compared to Lite, provides continuous Real-Time iEEG, the ability to perform on-demand iES, and more accurate synchronization at the expense of having more on-body equipment, while still relatively lightweight (~9 lbs). The additional latency and uncertainty associated with Mo-DBRS Lite (mean ± s.d., 432 ± 83 ms, Table 2) comes from the fact that the RNS Neurostimulator registers a *Magnet* event only every 500 ms. The synchronization of Mo-DBRS Lite, however, can be improved by observing a known neural response to specific stimuli (Rao et al., 2017) or with future hardware or software changes to the commercially available RNS Neurostimulator. Once a *Magnet* is detected, an iEEG data window is stored based on pre-programming that is modifiable by the user (30, 60, 120, 180, 240 s long) and with a fixed 2:1 ratio of data saved before and after the captured *Magnet*. Mo-DBRS Full is also capable of sending a *Magnet* command, which can be utilized as a backup method to recover data if Real-Time iEEG communication drops. Another limitation of Mo-DBRS Full is the relatively long latency (~1.4 s; Figure 2F) of the *Stim* command, which is limited by the capabilities of the RNS System, and is thus important to consider when implementing time-locked iES research studies. However, research studies that rely on closed-loop iES available in the commercially available RNS System to detect an iEEG feature (e.g., oscillatory band power or phase value) can avoid this latency limitation by pre-programming the RNS System to directly trigger iES based on iEEG activity. This option is available for users on the Programmer. In this case, iEEG detection latency ranges from ~0 to 128 ms, depending on the tracked iEEG frequency band. Latency associated with iES ranges from ~0 to 192 ms, depending on electrode impedance, battery depletion, and iES current. In total, closed-loop iES latency thus ranges between ~0 and 320 ms. There is also

an optional added delay that is configurable in order to target iES to an upcoming frequency phase (refer to NeuroPace, Inc. for details).

Security of the wireless connection

For researchers who enter into a collaborative agreement with a device company (e.g., NeuroPace or Medtronic), use an IRB approved protocol, and obtain participants' informed consent, the Mo-DBRS platform can provide temporary access to and programmable control over several aspects of the implanted device, all within the established limitations of the FDA-approved device. It is critical to further ensure the security of the added wireless connection associated with Mo-DBRS Full (see STAR Methods, Mo-DBRS Security section). Of note, for Mo-DBRS integration, the RNS System is not modified to remove any password controls nor is any direct communication with the RNS Neurostimulator possible outside of the FDA-approved Programmer-Wand-Neurostimulator interface.

Ethical Considerations

Patients with implanted RNS Neurostimulators often have long periods of time (e.g., months) during which therapy is not enabled for clinical reasons (e.g., evaluation of candidate iEEG signals for therapy), during which research-related studies can be completed. Participants can also consent to have therapy temporarily withheld during an Experimental Task Paradigm. Alternatively, careful selection and recruitment of participants with a historically lower frequency of treatment events (i.e., daily iES deliveries) or completion of research studies during optimal times given circadian and/or multidien rhythms in clinical symptoms (Baud et al., 2018) may further reduce the presence of confounding treatment-related iES events during research studies. In our experience, this approach has resulted in very rare therapy-related instances of iES (~0.03% of iEEG data affected in only 1 participant).

Added risks related to iES are minimal since stimulation charge densities used in research are usually much lower (<10 $\mu C/cm^2$, Suthana et al., 2012; Suthana et al., 2018) than what is typically used clinically for example in epilepsy treatment (maximum RNS System charge density that can be delivered is 25 $\mu C/cm^2$). In order to minimize risks, a clinician (e.g., neurologist) should view iEEG activity during iES sessions and iES should be set below the threshold that elicits after-discharges, monitored continuously, and immediately reduced if needed.

Participants should also be informed of risks related to battery drainage from Mo-DBRS-related research studies, which are minimal with respect to the RNS System's 4-year (RNS-300M) or 8-year (RNS-320) typical timeline for Neurostimulator replacement due to battery depletion. In other systems (e.g., RC+S), these risks are negligible given rechargeable battery capabilities. For the RNS System, the impact on battery life from *Magnet*-triggered iEEG storage is similar to that of treatment-related iEEG storage due to patient *Magnet* swipes. Battery impact due to iES in a typical research study is similar to or lower than ongoing clinically-programmed responsive neurostimulation therapy, the impact of which is further reduced by the use of lower iES current settings in research protocols. Real-time iEEG has more of an impact on battery life, where 1-hour of research equates to

approximately 10 hours of battery life. Given the widespread use of implantable neurostimulation devices, there are a number of potential research candidates (> 2000) and thus, each participant's time commitment can be limited to reduce impact on battery life (e.g., 1–2 days out of the 4/8-year timeline). Altogether, ethical considerations related to withholding of treatment, iES, and battery drainage should be discussed with and approved by an IRB, communicated to the participant during informed consent, and considered during study design and the participant recruitment process.

Mo-DBRS compatibility with other implantable devices

The Mo-DBRS platform is designed for the NeuroPace RNS System since it is the closed-loop neurostimulation system currently implanted in the largest population (>2000 patients with average quarterly implants exceeding 150), while other systems emerge (e.g., Medtronic Summit RC+S), which are currently implanted in a dozen or so patients (Stanslaski et al., 2018; Kremen et al., 2018; Gilron et al., 2020). The RC+S System allows for semi-continuous iEEG recording and hardware/software resources for closed-loop iES. It also has Bluetooth remote connection capability and an application programming interface (API) that allows for development of custom software for device control. While not all Mo-DBRS Research Tools are necessary for utilizing the RC+S system for research, the RP, wearables and associated Experimental Computer and Task Paradigm scripts can be integrated to expand the RC+S System functionality for use in a broader array of research studies.

Devices such as an RP provide an opportunity for development of hardware and software solutions that can integrate multiple wearables with an implanted system. Future studies should investigate whether the Mo-DBRS platform can be integrated with the RC+S System by having the Clinician Telemetry Module (CTM, Stanslaski et al., 2018) connected with the RP via a USB connection. This would likely shorten the Bluetooth transmission latency for communication with the external control interface, while still allowing remote access over the network for necessary commands. Synchronization of iEEG with wearables would also likely be improved since Mo-DBRS external hardware is used for alignment. Future studies should also investigate whether an electromagnet device can be used for synchronization with other implantable devices. The RC+S System does not have a *Mark* synchronization option and instead relies on internal pulse generator timestamps. The absence of a reference signal (e.g., *Mark*) can pose a challenge for synchronization with externalized data due to clock drifts. In such cases, the ground truth can only be established by using simultaneous events (e.g., *Marks* or *Magnets*) that can be observed in the different data streams.

Mo-DBRS Use Cases

Neuroscience-related research on behaviors that involve naturalistic body and/or head movements, such as walking, driving, eating, and socializing, is uniquely suited for studies using the Mo-DBRS platform. Furthermore, Mo-DBRS studies with patients who suffer from movement-related disorders (e.g., walking/driving in Parkinson's disease, dystonia), loss of control (e.g., eating), obsessive-compulsive disorder (e.g., compulsions), and post-traumatic stress disorder (e.g., trauma-related memories) are now possible given clinical trials that are ongoing in these patients using implantable closed-loop neurostimulation

devices (ClinicalTrials.gov NCT04011449, 2019; NCT03582891, 2018; NCT04152993, 2019). Patients with significant comorbidities (e.g., severe movement impairments) may be unable to wear the Mo-DBRS Research Tools on-body, in which case Mo-DBRS Lite or Mo-DBRS Full stationary setups may be more suitable. Research planning should involve careful selection of individuals depending on the study's needs and a participant's capabilities. With increasing use of chronically implanted closed-loop neurostimulation systems within a variety of deep brain regions, collaborative and multi-institutional studies will be in a unique position to optimize the design of future Mo-DBRS-related studies in the fields of Cognitive and Clinical Neuroscience.

STAR METHODS

RESOURCE AVAILABILITY

Lead Contact—Further information and requests for resources should be directed to and will be fulfilled by the Lead Contact, Nanthia Suthana (nsuthana@mednet.ucla.edu)

Materials Availability

The code, data and materials for the re-creation of the Mo-DBRS platform as well as suggested solutions for proper use, setup, and synchronization of data streams are publicly available at GitHub repository (https://github.com/suthanalab/Mo-DBRS).

Data and Code Availability

The code is open-source and can be downloaded from GitHub repository (https://github.com/suthanalab/Mo-DBRS). Further data is available from the corresponding author upon reasonable request.

EXPERIMENTAL MODEL AND PARTICIPANT DETAILS

We implemented the Mo-DBRS platform in-vivo in seven participants previously implanted with the RNS Neurostimulator (Table S1) for treatment in accordance with the product labeling and ex-vivo (benchside) with a test RNS Neurostimulator. For in-vivo tests, all participants volunteered for the study by providing informed consent according to a protocol approved by the UCLA Medical Institutional Review Board (IRB). To avoid unintended stimulation artifacts in the iEEG activity, responsive neurostimulation therapy was not enabled during experimental sessions, given the participant's informed consent to do so. Neuropsychological scores for each individual were determined using known and previously reported methods (Suthana et al., 2015) (Table S2).

METHOD DETAILS

Mo-DBRS Components and Setup

Intracranial EEG (iEEG) Data Acquisition: The FDA-approved RNS System (Figure 1A) includes an implantable neural device (RNS Neurostimulator) used to detect abnormal electrical activity in the brain and respond by delivering imperceptible levels of electrical stimulation to normalize brain activity before an individual experiences a seizure. Each participant with an RNS System has one or two implanted lead(s) that are 1.27 mm in

diameter, each with four platinum-iridium electrode contacts and an electrode spacing of either 3.5- or 10-mm. To localize electrode contacts to specific brain regions, a high-resolution post-implantation CT image is obtained and co-registered to a pre-implantation whole brain and high-resolution MRI for each participant using previous methods (Suthana et al., 2015) (Example Figure 1B). The RNS System records iEEG activity on up to four bipolar channels at 250 Hz. Onboard Analog filters (FFT magnitude spectrums Figures S6, S7) can be configured to capture the widest possible bandwidth 4 – 120 Hz for the RNS-300M or 1 – 90 Hz for the RNS-320 models. The analog filter is 1st order Butterworth bandpassed with a 3 dB amplitude attenuation at the cutoff frequencies. If necessary, the real amplitude levels of the neural signal at the out-of-range frequencies close to cutoffs can be estimated using a 1st order Butterworth transfer function. We verified the filter transfer function with the test RNS-300M with low frequency single tones and obtained the amplitude attenuation results: 4 Hz – 0.71, 3 Hz – 0.60, 2 Hz – 0.42. The acquired iEEG data can be stored in real-time (Real-Time iEEG) or transferred at a later time (*Magnet*-triggered iEEG) to a Laptop or Tablet Programmer device (see the *Mo-DBRS Research Tools* section below for details). To view Real-Time iEEG activity on the Experimental Computer, a Virtual Network Computing (VNC) TightVNC server was installed on the Laptop Programmer, running while placed in the participant's backpack. Until VNC can be supported on the Tablet Programmer, a phone camera stream can be transmitted and used for viewing the real-time data (Figures S3D).

Virtual and Augmented Reality (VR/AR): The Mo-DBRS platform currently enables successful synchronization with VR/AR headsets equipped with eye-tracking, including the SMI modified Samsung gear VR, TOBII HTC Vive, Microsoft HoloLens, Magic Leap and can be adapted for use with other VR/AR headsets. VR/AR environments are programmed using openly available 3-D modeling and game development tools such as the Unity game engine and the C# language, to implement customized immersive environments with controlled stimuli and functionalities. Using motion capture (wearable or wall-mounted cameras), the participant's location can be mirrored in real-time in the VR/AR application. Example code for this implementation is openly available on GitHub (https://github.com/suthanalab/Mo-DBRS).

Biometric Measurements: Simultaneous Photoplethysmogram (PPG), electrodermal activity (EDA), electrocardiogram (ECG), and respiration (RSP) measurements can be performed using the wireless and wearable Smart Center system (BIOPAC® Systems, Inc.), controlled by the Acq*Knowledge* software interface. The Mo-DBRS platform integrates the BioNomadix Smart Center device, a digital interface with a USB connection, that collects data from two BioNomadix (Figure 3D) transmitters (First: RSP + ECG; Second: PPG + EDA). The USB-TTL Interface module can be used for millisecond accurate TTL synchronization through a USB serial port.

The setup uses three ECG recording electrodes fixed to the left and right upper chest and one on the left lower chest. Two EDA recording electrodes can also be placed on the tips of non-dominant hand fingers (Figure 6C). The BioNomadix and USB-TTL interface module is connected to acquisition modules and an Experimental Computer. Within the Biopac

Acq*Knowledge* software, which is run on the Experimental Computer, all recordings can be configured with a sampling rate of 2 kHz. The Biopac acquisition software can run throughout the experimental session, and the data can be synchronized with the iEEG data and other recordings from the Mo-DBRS platform offline.

Eye-tracking: Many VR/AR headsets currently have built-in eye-tracking (e.g., SMI modified Samsung gear VR, TOBII HTC Vive, Microsoft Hololens, Magic Leap), which is automatically synchronized with the VR/AR tasks (for example programmed in the Unity game engine). For real-world tasks in naturalistic environments, the lightweight Pupil-Labs eye-tracking device (Pupil Core headset, Kassner, Patera, and Bulling, 2014) can be used, which has an open-source platform for pervasive eye-tracking and mobile gaze-based interaction -- providing binocular eye cameras (up to 200 fps), and an external world-view camera (up to 120 fps) (Figure 3C). An Experimental Computer can control the eye-tracking hardware through ZeroMQ asynchronous messaging over a local network. The Pupil-Labs mobile application and an Android phone that controls the head-mounted eye-tracking device can be used for ambulatory tasks, whereas a direct connection is sufficient for stationary tasks. The Pupil Capture plugin manager can be configured to include: Annotation Capture (software synchronization marks), Blink Detection (online blink detection algorithm), Pupil Remote (allows wireless eye-tracking control and streaming), Time Sync (for network clock synchronization). For calibration, we used the Screen Marker Calibration and Accuracy Visualizer to assess its quality.

Scalp EEG: Participants with chronically implanted neural devices can also wear a scalp EEG cap that allows for ambulatory behaviors. We integrated, with the Mo-DBRS platform, a mobile 64-channel scalp EEG system (Wave Guard and eego™ mylab system, ANT Neuro, The Netherlands) that includes a lightweight amplifier (~ 2 lbs) which connects to the EEG cap and a small tablet to which data is being transmitted, and which can both be carried in a backpack. For electrode digitization and localization, we used ANT Neuro's xensor™, a system for real-time EEG electrode pinpointing, digitization, and visualization based on infrared high-accuracy measurements (< 2 mm accuracy). Measurements were performed using a pointer and reference tools (infrared-reflective objects) relative to the head and underlying brain (if MRI was available). Accuracy was further improved by using xensor's built-in feature for individual head shape generation (ANT Neuro, 2018). Scalp EEG and iEEG data were then synchronized (see the Mo-DBRS Synchronization section below) and analyzed offline.

Mo-DBRS iEEG Research Tools—Flexible control over the implanted RNS Neurostimulator, real-time iEEG recording and storage, iES delivery, and synchronization of data streams during free movement require additional tools that the user can re-create. These Research Tools are listed below, some of which come with the commercially available RNS System and others that can be provided by NeuroPace upon request or built by the user using the circuit and software code details provided here. Previous studies (Aghajan et al., 2017; Meisenhelter et al., 2019; Henin et al., 2019; Rao et al., 2017) have used variations of the Programmer, Programmer Tool, Wand, Wand Tool, and Electromagnet.

Experimental Computer: Any experimental device (e.g., laptop, desktop or phone) that runs the behavioral or cognitive task of interest (Experimental Task Program) and sends commands over the network to remotely control the RNS System (Figure 1D).

Programmer: A Programmer (Laptop or Tablet version) that comes with the commercially available RNS System can be used to retrieve, store, and monitor Real-Time iEEG as well as trigger delivery of iES (Figure 1D). The Laptop Programmer is only compatible with the older RNS-300M model (discontinued by NeuroPace), and the Tablet Programmer is compatible with both the older RNS-300M and newer RNS-320 models. The Tablet Programmer does not require the researcher to manually program data storage commands (i.e., using the *Store* command, see the Programmer Tool section below) into the Experimental Task Program (see GitHub link for example code), unlike the Laptop Programmer, since Real-Time iEEG data storage on the Tablet is performed automatically in chunks of a predefined duration (programmable by the user) between 60 seconds and 90 minutes. Lastly, the Tablet Programmer is more responsive and thus delivers commands to the implanted RNS Neurostimulator faster (see the Mo-DBRS Characterization and Validation section) compared to the Laptop Programmer.

Programmer Tool: To control the Programmer's graphical user interface (GUI), a Programmer Tool, or Arduino SAM Board (Model "Due", 32-Bit ARM Cortex-M3) can be used, which accepts one ASCII byte from the Experimental Computer and forwards the information to the Programmer or Wand Tool (Figure 1D). The Programmer tool can be provided by NeuroPace upon request. There are two firmware versions for the Programmer Tool, one compatible with the Laptop Programmer and the other one with the Tablet Programmer. The Laptop Programmer Tool allows for a trigger of four valid commands on the Programmer: 1) The *Store* command stops Real-Time iEEG transmission, stores up to 240 seconds of previously observed data, and then starts Real-Time iEEG again via a mouse click that selects related functions within the Laptop Programmer GUI. 2) The *Stim* command initiates the Laptop Programmer to trigger the delivery of iES under predefined parameters that can be manually set by the user on the Laptop Programmer. 3) The *Mark* command delivers a timed and visible pattern into the Real-Time iEEG recording, allowing synchronization with externally acquired data. Specifically, the *Mark* command triggers the Wand Tool to inject a distinctive noise pattern, 64 ms in duration, into the Real-Time iEEG data (Figure 2A) that can be analytically distinguished from the ongoing neural signal (see the Mo-DBRS Synchronization section below). 4) The *Magnet* command delivers a 520 ms wide electromagnetic pulse (Figure 2B), which triggers iEEG storage on the implanted RNS Neurostimulator. This command allows an alternative way of storing the iEEG data through the Wand Tool that does not require real-time transmission to the Programmer. However, if using the *Magnet* command to trigger data storage, the iEEG data needs to be externally downloaded (by interrogating the implanted RNS Neurostimulator via the Wand) before it gets overwritten by another *Magnet* command (given the RNS System's limited on-device storage space). The RNS-300M (RNS-320) model can store up to 7.5 (13) minutes of Magnet-triggered iEEG data (from 8 electrodes, 4 bipolar recordings). The RNS System data buffer capacity is increased if recording on fewer channels (e.g., up to 30 minutes [RNS-300M] and 53-minutes [RNS-320] recordings on 1 bipolar channel). The Tablet

Programmer Tool provides a broader range of possible controls in addition to the described four commands enabled with the Laptop Programmer. Specifically, there is added support for: RNS-300M/RNS-320 mode selection, independent Real-Time iEEG start/stop commands, and software labeling for synchronization and other purposes.

The Programmer Tool's input is a USB serial connection (baud rate: 9600 bps Laptop Programmer Tool, 57600 bps Tablet Programmer Tool). It has two outputs, an output USB connection towards the Programmer and a proprietary NeuroPace connection towards the Wand Tool (described below, Figure 1D). The Programmer Tool is powered with the input USB connection or a 12 V battery (required for *Magnet* commands).

Wand: The Wand is a device that comes with the commercially available RNS System that every patient has in their possession and is used to communicate wirelessly with the implanted RNS Neurostimulator via Near Field Telemetry when placed on the surface of the head (Figure 1D).

Wand Tool: The Wand Tool is a device that holds the Wand and produces the command triggered *Mark* pulses for Real-Time iEEG synchronization and *Magnet* pulses for Magnet-triggered iEEG storage (Figure 1D). The Wand Tool is not part of the commercially available RNS System but can be provided by NeuroPace upon request.

Wireless Control Device (Raspberry Pi): All of the previously described Research Tools can be used for stationary (tethered) laboratory computer-based Experimental Task Programs. However, to enable a completely wearable solution that allows for free movement such as during spatial navigation of VR/AR or real-world environments, a small single-board computer, such as the Raspberry Pi 3 (RP, Figure 1D), Model B, running Raspbian GNU/Linux 9.9 (Stretch) distribution, can be used as a wireless bridge between the Experimental Computer and Programmer Tool. This wireless control device can be built and customized by the user based on the details provided. The RP was chosen because it satisfies the minimal requirements: onboard wireless (e.g., network controllers, Bluetooth, or others) and USB peripherals. Wireless communication relies on a lightweight publish-subscribe network protocol MQTT v5 (Message Queuing Telemetry Transport) running over a Transmission Control Protocol (TCP) and Transport Layer Security (TLS). Basic RP functionality involves running a local, secure MQTT broker that reroutes messages from the Experimental Computer Client to an RP client, which further forwards commands from the Experimental Computer to the Programmer Tool. The communication between the RP and the Experimental Computer is centered around the MQTT broker running on the RP. The security of this connection was handled using the MQTT with a TLS security and x509 client certificates for authentication. On the RP we generated a local certificate authority, MQTT broker, and server/client x509 certificates signed by that authority. The server and client certificates were used for securing the RP MQTT broker, the RP MQTT client, and the Experimental Computer MQTT client, respectively. The custom shell script (see GitHub) was used to perform these steps directly on the RP, after which the client certificates were securely transferred (direct, wired connection) to the Experimental Computer. In this process, we used OpenSSL v1.1.1, an open-source toolkit for TLS (v1.2) protocols. With valid certificates, this resulted in an encrypted pipeline (Experimental Computer Client – RP

Broker – RP Client) through which the messages could flow securely. Mo-DBRS supports one connection at a time with trusted clients who have the signed certificate. If tasks are completed in indoor environments, the RP can be configured with a static IP address and connected to a local wireless network. We have used the Asus RT-AC5300 router; we suggest using this router or one with similar performance. For tasks in outdoor environments, the RP can be configured to provide a remote Access Point (Wi-Fi hotspot) (Raspberry Pi Foundation, 2017). If not explicitly stated otherwise, all example scripts (GitHub) on the RP were written in Python 2.7 and C, and are available for download. Once the connection is established, the server can be put into an idle state (i.e., blocking the read call function) until a command from the client is received. When the acknowledge receipt is received back from the Programmer Tool, a timestamp is logged. Experimental Computer timestamps are also logged before each command, which can be later used to verify synchronization methods. The role of the RP is critical in the following cases: 1) During the Experimental Task Program, the RP is the only communication channel between the Experimental Computer and the Programmer Tool–this connection is necessary to send behaviorally relevant commands to the Programmer Tool; 2) When the Experimental Task Program requires complex command sequences and their delivery at specific times with high precision. In general, partial implementation of these functions at the RP level, rather than on the Experimental Computer, warrants better flexibility and accuracy of timing; 3) When the Experimental Task Program can be entirely implemented on the RP and, thus, the RP can serve the role of the Experimental Computer.

Telemetry Switch: Since the RNS Neurostimulator is a chronically implanted neural device with no externalized wires, it is possible to simultaneously record scalp EEG synchronized with iEEG (see the Mo-DBRS Synchronization section for details). However, telemetry associated with Real-Time iEEG results in noisy scalp EEG data, due to placement of the scalp EEG cap in between the Wand and the implanted RNS Neurostimulator. We therefore provide solutions for noise reduction in the simultaneously recorded scalp EEG. The first solution is the use of the Magnet command to trigger iEEG storage, which does not require telemetry and thus results in artifact-free scalp EEG data. However, this method suffers from poor synchronization accuracy (> 250 ms) associated with the Magnet command relative latency. A second solution can be used is to programmatically switch on/off telemetry (using a Telemetry Switch, via a USB connection) to prevent associated artifacts when telemetry is not needed. This can be implemented by manually unplugging of the Wand USB cable from the Programmer, which would be impractical and prone to errors. Thus, we built a custom Telemetry Switch that can be placed between the Programmer and the Wand (Figure 1D) to enable/disable telemetry when needed (i.e., enabled when sending commands) by controlling the digital input connected to the RP. If scalp EEG is not needed, the switch may remain ON. The telemetry switch can be built and customized by the user based on the circuit details provided (see Figure S4G–H) and code (GitHub). Telemetry Switch usage is described in the section on Scalp EEG Artifact Reduction – Telemetry Switch. If telemetry is required, artifact rejection methods can be used offline after data acquisition (see the Scalp EEG Artifact Reduction – Offline Processing section).

Electromagnet: The Mo-DBRS Lite version of the platform can be used as an alternative solution to the full Mo-DBRS platform, through the use of the custom-built experimental electromagnet device, which, due to its size, is a more lightweight solution and thus comfortable for participants who may be physically impaired and/or have limited mobility. The Mo-DBRS Lite platform requires an electromagnet device that produces a pulse with a minimum duration of 520 ms (anything shorter will not be registered by the implanted RNS Neurostimulator) that can be triggered by the custom-built battery-powered wearable control box (see Figure S1 for circuit details required to reproduce the control box). The electromagnet component (Figures S1B–C) is not part of the commercially available RNS System, rather it is a Research Tool that can be provided by NeuroPace upon request. Depending on a predefined length of Magnet-triggered stored iEEG data specified by the user in the Programmer prior to the experimental session, the electromagnet device can be set to be triggered at predefined configurable time intervals (e.g., 30/60/90/180 or 240 s in our case). A small LED—located at a proximity of the electromagnet—can be configured to turn on simultaneously with the triggered electromagnetic pulse, and thus be captured by external or wearable cameras, which can later be used to synchronize iEEG activity with external data. Manual triggering of the electromagnet and timers can be handled using a PIC controller (see assembly code on GitHub) that requires additional circuitry for power amplification to drive the electromagnet (Figures S1A,B). For remote and programmatic control of the wearable electromagnet device (including pulse duration and time of delivery), additional circuitry can be added to the RP (see Figures S1A,C for full details needed to reproduce).

Mo-DBRS Security—It is critical to ensure the security of the added wireless connection associated with the Mo-DBRS Full platform. First, the security of the router and created local network should be set up with strong credentials, firewall, encryption, and disabled internet access if not required for the study. Second, standard security procedures, such as strong password protection, should be used for each device, most importantly, for the Experimental Computer and RP. Third, the connection between the Experimental Computer and RP should be established using client authentication and encryption. For this, we provide a solution in the form of certificate authentication, which provides an encrypted communication channel (see Wireless Control Device (Raspberry Pi) section in STAR Methods for details).

Mo-DBRS Characterization and Validation

In-vivo testing: Seven participants wore the Mo-DBRS platform and maneuvered freely through an indoor environment, where wall-mounted motion capture cameras were used to monitor position and full-body movements with submillimeter precision (Figure 3B). Eye position and movements were recorded with the Pupil Core eye-tracking headset (Figure 3C) worn and carried with the Pupil Mobile phone device inside of a wearable backpack (Figure 1C, Figure 6A). Heart rate (ECG) was measured from the participant’s chest, and skin conductance via sensors from the fingers (Figures 3A,D, Figure 6C). Participants also wore a scalp EEG cap and were asked to carry a sturdy backpack in which we placed necessary equipment (e.g., Mo-DBRS Research Tools, scalp EEG amplifier, and data acquisition tablet). Participants were able to wear the setup comfortably for several hours throughout the

day. The Wand and Wand Tool were tightly strapped together with a 'Wand holder' (iPhone holder was used; Figure 1C, Figure 3A, Figure 6A) using Velcro tape and a rubber band to ensure a stable connection and prevent misalignment between the Wand and Wand Tool, which if not done correctly would have led to missed *Marks*. The flexible metal Wand holder was secured to the backpack to relieve the weight of the Wand and Wand Tool on the participant's head and to provide stability and movement flexibility. Lastly, the Wand was angled close to the implanted RNS Neurostimulator location. Once Real-Time iEEG telemetry was established, it was fixated to the scalp EEG cap using Velcro tape placed on the side of the Wand Tool that was secured to the participant's head (Figure 1C, Figure 3A, Figure 6). We tested both the full Mo-DBRS and Mo-DBRS Lite versions of the platform, which differed in how iEEG data was handled (see Table 2 and the Mo-DBRS Lite section). Mo-DBRS uses the *Store* command to save streamed Real-Time iEEG on the Programmer (Figure 3E) and the *Mark* command for synchronization. The Mo-DBRS Lite version, on the other hand, uses the *Magnet* command to save iEEG on the implanted RNS Neurostimulator and the same *Magnet* command for offline synchronization. In parallel, the Experimental Computer (Figure 3G) acquires other streams of data by running the Experimental Task Program (e.g., in Matlab or Unity), eye-tracking software, motion capture software, and biometric measurements (Figures 3B–D). The Experimental Task Program controls the flow of the experiment based on collected streams of data in real-time. Closing the loop toward the participant in order to control a VR/AR environmental scene, depending on the body and head position, can be achieved by updating the VR/AR headsets (Figure 3H) or sending Audio/Video messages in real-time. Equipment can be connected through a local wireless network, allowing real-time control, storage, streaming (Figures 3B–F – communication on the left), and synchronization (Figures 3B–F – recordings and synchronization on the right) with the uncertainty of below 16 ms for the Mo-DBRS Full platform version. The synchronization fixation points are *Mark* events for the Mo-DBRS Full platform and *Magnet* events when using the Mo-DBRS Lite version.

All commands were sent from the Experimental Computer using Unity software (see GitHub for example code). After the experimental session, all data is then collected, synchronized, and scalp EEG can be cleaned using the methods described in the *scalp EEG Telemetry Artifact Rejection* section. Continuous recordings from all wearables were performed while participants were walking freely inside the room; simultaneous *Mark* signals were sent to all data streams with respect to the stored iEEG data. Synchronization signals (*Marks*) were sent 1 s after a *Store* command and 1 s before the next *Store* command.

Participants 1–5 and 7 freely walked through the room while iEEG and wearable recordings were performed. In Participant 6, Mo-DBRS Full was used to record simultaneous iEEG, body/head motion, and eye tracking during a spatial navigation task in which they were instructed to walk towards wall-mounted signs (Figure 5 and Video S1).

During separate sessions for Participants 1–5, we also characterized the reliability of Mo-DBRS commands (*Store, Stim, Mark*, and *Magnet*) using the Research Tools and in the following order:

- *Mark* and *Store*: 2 × 240 s iEEG blocks (via *Store* command) with 100 *Mark* commands each, delivered every 2 s.
- *Store, Magnet*, and *Stim*: 3 × 240 s iEEG blocks (via *Store* and *Magnet* commands) each with 16 iES pulses (*Stim* command) with 100 ms burst duration, 0.5 mA output current, each at every 1.8 s, 2 s, and 2.2 s.
- *Store, Magnet*, and *Stim*: 3 × 240 s iEEG blocks (via *Store* and *Magnet* commands) each with 16 iES pulses (*Stim* command) with 2000 ms burst duration, 0.5 mA output current, each at every 3.8 s, 4.2 s, and 5 s.
- *Store, Magnet*, and *Stim* with the Telemetry Switch: 2 × 240 s iEEG blocks (via *Store* and *Magnet* commands) each with 8 iES pulses (*Stim* command) with 100 ms burst duration, 0.5 mA output current, done with the Telemetry Switch on/off, $t_0 = 5$ s; $t_1 = 7$ s; $t_2 = 3$ s; $t_3 = 5$ s (for t_i definitions see the Scalp EEG Artifact Reduction – Telemetry Switch section below).
- *Store, Magnet*, and *Stim* with telemetry switch: 1 × 240 s iEEG block (via *Store* and *Magnet* commands) each with 16 iES trials with 100 ms burst duration, 0.5 mA output current, done with the Telemetry Switch on/off, $t_0 = 4.8$ s; $t_1 = 3.9$ s; $t_2 = 0$ s; $t_3 = 5$ s.

Ex-vivo testing: Latency measurements were performed on a test RNS-300M Neurostimulator (bench-side ex-vivo). The same set of commands was sent as in the in-vivo studies, but instead sent from the RP instead of the Experimental Computer. Command delivery triggered from the RP and the corresponding absolute latency were estimated by executing a send function while simultaneously changing the state of the RP's General-Purpose Input-Output (GPIO) pin. The command delivery could be directly observed on the test RNS-300M device's recording contacts and compared with the RP's GPIO output using an oscilloscope. Execution of the *Stim* and *Store* command could be observed directly on the recording contacts of the test RNS-300M device. For measuring absolute latencies of the *Mark* and *Magnet* commands, a test coil with two turns and a resistor was placed in between the Wand and the test RNS-300M device. The timing of the generated voltage across the resistor was then measured with respect to the RP GPIO.

For measuring relative latencies, a Reference Pulse was generated on the RP's GPIO pin, attenuated from 3.6 V to 2.6 mV using a resistor divider, recorded by analog front-end, filtered, and digitized (250 Hz sampling) into the Real-Time iEEG (Figure S2A). We observed the delivered Reference Pulse and command (Magnet and Mark) artifacts directly in the Real-Time iEEG, which was stored via the Store command (implemented on the Programmer). Finally, we compared the Real-Time iEEG events with initiation timestamps from the RP to measure the relative latencies.

Due to different clocks on the test RNS-300M device and external wearable equipment, the RP timestamps and RNS timestamps were synchronized by aligning the first *Mark* artifact that appeared in both recordings and setting the RP 1/f clock slope to be the linear fit of the RNS clock slope. Effectively, this resulted in an adjustment of the RP timestamps by a ratio

of the clock mismatch between the test RNS-300M and RP (a similar method was used in Meisenhelter et al., 2019).

Network round-trip latencies between the Experimental Computer and the RP were measured directly in code using time libraries on the RP (i.e., Python and C language). The Asus RT-AC5300 Wireless Router was used to provide a reliable connection within the range of 20 meters.

Mo-DBRS synchronization—We detail here an example solution for utilizing the *Mark* command for synchronization. Specifically, *Marks* are delivered right after the *Store* command. At the same time, the Real-Time iEEG data is viewed in real-time to detect any loss of telemetry (Wand connection with the implanted RNS Neurostimulator), in which case the corresponding Real-Time iEEG data can be discarded. *Marks* are then detected using cross-correlation (no normalization) between iEEG data and each of 4 *Mark* signal templates, including a 3-spike template (Figure 2A) and three versions of a 2-spike template (if 1 of the 3 spikes are missing). *Marks* are identified as the time points where the correlation coefficient between the iEEG data and at least one of the four *Mark* templates is higher than 90% of the maximum determined correlation coefficient. These time points are then used to verify that the corresponding iEEG signal value is at a minimum (maximum absolute value of a signed 10-bit iEEG sample is 512) at the same time points. This cross-correlation procedure is repeated for the three versions of the 2-spike *Mark* template in cases where the full 3-spike *Mark* signal was not captured completely. The *Marks* that are detected using these 2-spike templates are appropriately shifted in time to account for the missed spike given that the predicted time between *Mark* template spikes is known. Using this method, we were able to detect all delivered *Mark* signals in the Real-Time iEEG that contain at least 2 spikes. For synchronization of Magnet-triggered iEEG see the Mo-DBRS Lite section.

For synchronization with the eye-tracking system, ZeroMQ API provides annotations for eye-tracking synchronization (~ 10 ms accuracy) with other data streams. Software annotations can be delivered from the Experimental Task Program (running the behavioral paradigms) to the Pupil-Labs software (Pupil Capture), which runs in parallel on the Experimental Computer. Annotation makers can be sent to the Pupil-Labs software each time the *Mark* command is sent to the implanted RNS System. Additional and redundant synchronization can be achieved by having a small LED placed on the edge of the outward-facing camera on the eye-tracking headset that can turn on for a short period of time (50 ms) simultaneously with the *Mark* command. The LED can be connected and controlled by the RP.

Synchronization, monitored by the Experimental Task Program (Figure 3, Figure S3A), is summarized as follows:

- Depending on the task, the iEEG, biometric measurements, and eye-tracking data can be synchronized using simultaneous *Mark* commands sent by the Experimental Task Program.

- iEEG/scalp EEG data can be synchronized with a *Mark* (or *Magnet*) command in the Mo-DBRS (Mo-DBRS Lite) platform.
- Due to pipeline delays with the eye-tracking software annotations, an LED indicator can be connected to the RP and turned on whenever a *Mark* or *Magnet* command is being received on the RP (Figure S3A). Similar to the electromagnet device, we used a 50 ms pulse from the RP to turn on an LED that was captured by the motion capture and eye-tracking cameras.
- All clock drifts were handled the same way as what was done with iEEG data (see Ex-vivo testing section). The data was aligned by matching the marking (*Mark* or *Magnet*) signals in all of the data streams and then subtracting the mean value of the relative latencies separately for all wearable systems. The worst-case standard deviation of all relative latencies between the various systems was used as the metric for assessing the total accuracy of synchronization.

There are two challenges in terms of synchronizing scalp EEG and iEEG data, as well as minimizing artifacts due to wireless communication with the implanted RNS System (see the Telemetry Switch section above). Synchronization can be done via the *Mark* or *Magnet* command, as the resulting signal patterns detected in the nearby scalp EEG electrodes are, in fact, beneficial and can be used to align the scalp EEG and the iEEG data streams. On the other hand, noise patterns resulting from iES or Real-Time iEEG transmission can be avoided using the Telemetry Switch or removed offline using signal processing methods (see the *Scalp EEG Telemetry Artifact Reduction* section below).

We performed referential recordings from all accessible channels in the scalp EEG, at 2000 Hz. A higher sampling rate was necessary to capture the full frequency range of the RNS Wand telemetry signals in order to model the artifacts that are later used in the cleaning procedure. The referential input signal range is up to 1000 mV_{pp}, which was again useful for capturing large telemetry artifacts and preventing amplifier saturation. For more information on the amplifier specification, see (ANT Neuro, 2018).

Scalp EEG data was processed and synchronized with iEEG data using Matlab 2018a with the Wavelet, Signal Processing, and DSP System Toolboxes. We first began with the raw, unfiltered scalp EEG data from all 64 channels sampled at 2 kHz, denoted as $\mathbf{R}_{C\times Nr}$ (C – number of channels; N_r – number of sample points per task). Each row of **R** was standard score normalized independently.

Next, we located the distinctive noise patterns (“synchronization artifacts”) that were created by either *Marks* (Figure 2A) or *Magnets* (Figure 2B), depending on whether the Mo-DBRS or Mo-DBRS Lite was used. To do this, we created *Magnet* $\mathbf{M}_{Nm}$ (N_m = 1040 points at 2 kHz) and *Mark* $\mathbf{T}_{Nt}$ (N_t = 128 points at 2 kHz) templates using scaled absolute values of their respective waveforms (e.g., Figure 2B, and Figure 2A). Similar to the *Mark* detection in Real-Time iEEG, exact positions of the artifacts were extracted using raw cross-correlation with no normalization between each channel’s time series and templates. For positive side coefficients:

$$\rho_{c,m} = \sum_{n=0}^{N_r - m - 1} \frac{R_{c,n+mT}}{M_n}, m = 0, \ldots, N_r - 1$$

Out of 64 channels, 10 with the highest scaling factor (i.e., s.d.) were chosen for the synchronization artifact detection due to their proximity to the Wand. Since artifacts across the channels vary only in amplitude, it is best to detect from those with the highest artifact to signal ratio. Additionally, we made three assumptions: 1) each of the 10 selected channels contained all of the delivered *Marks* or *Magnets*, 2) within a single channel the *Marks* and *Magnets* all had the same amplitude, and 3) the scalp EEG signal amplitude during *Magnets* and *Marks* was significantly larger than at any other times, including periods of Real-Time iEEG transmission. In practice, *Magnet* scalp EEG artifacts (Figure S4B) have the largest amplitude, followed by *Mark* scalp EEG artifacts (Figure S4A). Based on these assumptions, we chose a threshold of 10% lower than the maximum observed correlation per channel. This automated method for synchronization had a 98% success rate. It was confirmed by using manual inspection of 3 sample scalp EEG/iEEG datasets and comparing it to the RP time logs of command delivery as ground truth. The incorrect 2% were all false positives that identified some of the telemetry artifacts as *Marks*. Example figures showing artifacts in scalp EEG used for synchronization can be found in Supplementary Information (Figures S4A,B,C).

As each *Magnet* command saves 2/3 of the chosen iEEG data before and 1/3 after the *Magnet* event, we extracted 160 s before and 80 s after the detected *Magnet* timepoint in the scalp EEG data (in this case of pre-configured 240 s Magnet iEEG storage duration). The rest of the data was discarded, and a new scalp EEG matrix $\mathbf{S_1}_{,T\times C\times Ns}$ (T – number of trials; C – number of channels; N_s – number of sample points per each 240 s block, e.g., 2000 Hz × 240 s) was synchronized with stored Magnet-triggered iEEG data. When Real-Time iEEG was used, we sent a *Mark* command 1 s before and after the *Store* command. Scalp EEG data in between two detected *Marks*, ~238 s apart, was extracted as one trial dataset and turned into the same scalp EEG matrix $\mathbf{S_1}_{,T\times C\times Ns}$ (N_s –2000 Hz × 238 s), aligned with the Real-Time iEEG data. Lastly, resulting matrices were again standard score normalized per channel. If the *Stim* command was used, iEEG data (stored via *Store* or *Magnet*), could also be synchronized by manual detection of iES artifacts in iEEG and scalp EEG. Of course, this synchronization is only feasible when iES artifacts are present in the scalp EEG data (Figures S4C,F).

Scalp EEG Artifact Reduction

Telemetry Switch: We tested the functionality of the Telemetry Switch, which enabled telemetry communication at specific time points, for instance, when sending a *Store*, *Stim*, or *Mark* command (*Magnet command* does not need telemetry). Here, despite losing continuous Real-Time iEEG, a *Magnet* command can be used to store the iEEG data since telemetry is disabled. For example, we performed an experimental session that involved sending a train of iES bursts, which required cycles of On/Off telemetry. One iES cycle included enabling telemetry, which took t_0 seconds to get recognized by the GUI on the

Programmer (scalp EEG remains unaffected by telemetry until t_0). Once telemetry was enabled, the *Stim* command was sent, which required t_1 for delivery. Telemetry was then disabled for an arbitrary period of t_2 immediately after the iES was delivered, thereby providing clean scalp EEG data. The last relevant timing parameter was the time between the iES cycle preceding the triggering of data storage (t_3) (Figure S4D). This operation resulted in synchronized iEEG/scalp EEG recordings (Figures S4E,F). The procedure for sending other commands was done in a similar manner by enabling telemetry (same t_0) and varying t_1 values.

Minimal timings were determined in in-vivo experiments. The experimental telemetry switch was tested and used to partially prevent contamination of scalp EEG with telemetry-associated artifacts. Telemetry restart, stimulation, and Real-Time iEEG noise patterns were clearly present during the telemetry enabled state lasting t_1 (Fig. S4F, t_0 = 5 s; t_1 = 7 s; t_2 = 3 s; this sequence allows delivery of continuous stimulation every 15 seconds). Due to the inevitable delays in this pipeline, namely recognizing telemetry by the Programmer and iES delivery (t_0 + t_1), there was a lower limit for how often stimulation could be delivered reliably. We determined, empirically, that the minimal timing values were t_0 = 4.8 s, t_1 = 3.9 s, t_2 = 0 s, resulting in a total minimal stimulation period of 8.7 s using the Laptop Programmer. Values below this threshold caused either missed *Stim* delivery commands or rejections by the RNS System. The procedure for sending other commands was done similarly by enabling telemetry (same t_0) and varying t_1 values. It is worth noting that although the *Magnet* command could be used to synchronize scalp EEG with iEEG offline, *Mark* commands and Real-Time iEEG provide much higher accuracy (Fig. S2). Thus, for highly accurate synchronization with scalp EEG, telemetry-enabled blocks of Real-Time iEEG, containing *Marks*, should first be aligned with redundantly stored *Magnet* iEEG and then aligned with the scalp EEG using either stimulation or *Mark* signals captured in the Real-Time iEEG data. It should also be mentioned that the same method applies to the Tablet Programmer, except that the timings are expected to be somewhat improved.

Offline Processing: We provide here an offline solution for scalp EEG noise reduction to eliminate any artifacts that remain during enabled telemetry, such as: 1) Telemetry restart artifacts (Type I); 2) iES artifacts (Type II), and 3) and Real-Time iEEG artifacts (Type III) (Figure S4F). Type I artifacts appear as a series of alternating segments of two and three spikes, followed by a larger bi-spike (Figure S5A). Similarly, Type II artifacts consist of segments with two spikes, followed by a bi-spike (Figure S5B). Spike duration and their relative distance in time were deterministic and fixed– a property that was capitalized upon in our artifact rejection procedure (Spike: 4 samples; bi-spike: 16 samples at 2 kHz). Type III artifacts were spikes at 125 Hz (and harmonics) (Figure S5C).

Following the automated synchronization method for scalp EEG with iEEG, we normalized the *Magnet*/*Mark*-free scalp EEG $\mathbf{S_1}_{,T\times C\times Ns}$. To do this, we first flattened the input matrix to $\mathbf{S_1}_{,C\times(T\times Ns)}$ (in the same order as it came from the raw data in order to simplify analysis) and then applied the same technique to detect Type I and Type II artifacts as we did with *Magnets* and *Marks*. By observing scalp EEG recordings, we constructed binary templates $\mathbf{C}_{Nc}$ (N_c = 3174 points at 2 kHz) and $\mathbf{D}_{Nd}$ (N_d = 2824 points at 2kHz), following respective artifact waveforms from Figures S4F, S5A and Figures S4F, S5B. Note, that 3174 samples or

1.587 s of $\mathbf{C}_{Nc}$ template plus 2824 samples or 1.412 s of $\mathbf{D}_{Nd}$ template correspond to a portion of defined t_1 containing artifacts. With no *Marks/Magnets*, we made the same three assumptions used for synchronization and detected two types of artifacts using correlation. Again, for detection, we used ten channels with the highest physical proximity to the Wand. The manual inspection confirmed a 100% success rate in detection across 3 separate scalp EEG datasets, with RNS time logs of command delivery serving as the ground truth. Once the *Marks/Magnets* were detected, we extracted trials and exact sample points, resulting in matrices $\mathbf{A}_{Na\times C\times Nc}$ and $\mathbf{A}_{Na\times C\times Nd}$ (Figure 4A – 1 and Figure 4B-top) for the two types of artifacts (N_a corresponds to a number of detected artifacts per observed channel). We then applied PCA on scalp EEG N_c and N_d time series across all channels for each detected artifact separately, while skipping PCA application on adjacent channel pairs (O'Shea and Shenoy, 2018). The first 3 PCA components were sufficient to capture the artifacts' shape shared across different channels. We then eliminated clean scalp EEG during non-spike periods by point multiplication $\mathbf{PC}_{i,Nc} \times \mathbf{C}_{Nc}$ (and $\mathbf{PC}_{i,Nd} \times \mathbf{D}_{Nd}$) per each channel and each detected sequence, and applied vertical offset correction for each artifact spike so that it started from 0 (example Figure S5D). For each segment and channel, we fitted artifact templates to corresponding segments in **A** matrices and subtracted them from it (Figure 4A – 2). Using previously obtained synchronization timestamps, we reconstructed data into a matrix of original dimensions $\mathbf{S_2}_{,T\times C\times Ns}$. In order to clean Type III artifacts, we filtered each time series within the $\mathbf{S_1}$ matrix with a low pass Chebyshev Type I infinite impulse (IIR) filter of order eight and with a cut-off frequency of 125 Hz. We then downsampled data by a factor of 8 from 2 kHz to 250 Hz.

Further artifact rejection can be done using methods reported in Islam et al, 2016. In brief, we used a single channel artifact rejection algorithm in the time-frequency domain. First, the input 250 Hz sampled data were standard score normalized, and then Stationary Wavelet Transform (SWT) was performed (level = 10; Haar base wavelet). Artifact detection was done for approximation and detail coefficients separately. We examined D_8, D_9, D_{10}, and A_{10} coefficients for the input scalp EEG frequency band. Empirically determined thresholds detected outstanding discrepancy from scalp EEG's approximatively Gaussian distribution for each set of coefficients:

$$T_i = k_{A/D}\frac{\text{median}(|A/D_i|)}{0.6745}\sqrt{2\log N}$$

where N is the number of points in the input sequence and $k_A = 0.75$, $k_D = 5$. Coefficients identified as potentially containing artifacts were thresholded using the Garrote threshold function, after which inverse SWT was applied to reconstruct the cleaned signal. This method was applied to each Ns-point time-series within input $\mathbf{S_2}_{,T\times C\times Ns}$, resulting in output $\mathbf{S_3}_{,T\times C\times Ns}$ (Figure 4A – 3). For more details, see GitHub and Islam et al, 2016.

Finally, due to high pass filters with low cut-off frequency integrated into scalp EEG equipment, the presence of artifacts caused a voltage drift in raw data (visible slow transients on Figure 4A – 1,2,3). To account for this, we applied IIR high pass filter (order = 8; passband ripple = 0.2; cut-off frequency = 2 Hz) on $\mathbf{S_3}_{,T\times C\times Ns}$ resulting in clean scalp EEG matrix $\mathbf{S_4}_{,T\times C\times Ns}$ (Figure 4A – 4 and Figure 4B-bottom). To quantify the reduction of

artifacts, we calculated the root mean square value (RMS) for $\mathbf{S_1}_{,T\times C\times Ns}$, $\mathbf{S_4}_{,T\times C\times Ns}$, and portions of $\mathbf{S_1}_{,T\times C\times Ns}$ with clean scalp EEG. All RMS values were scaled with a maximum RMS value in $\mathbf{S_1}_{,T\times C\times Ns}$ for a given channel (Figure 4C, Figure S5E). Additional cleaning results can be seen in Figure S5F. Bad channels and channels not containing artifacts were omitted from processing. A total of 17 such channels in the presented case were detected visually and by having $\mathbf{S}_{C\times(T.Ns)}$ - $\mathbf{C}_{Nc}$ / $\mathbf{D}_{Nd}$ correlation of less than 0.1 on portions of scalp EEG already identified as artifactual. Correlation of less than 0.1 on portions of scalp EEG already identified as artifactual.

QUANTIFICATION AND STATISTICAL ANALYSIS

All analyses were performed using custom scripts in MATLAB. Details of analyses are reported in respective Method Details sections.

iEEG power spectrum extraction—All time-frequency power scalograms (Figure 5) were obtained using CWT (Continuous Wavelet Transform - MATLAB *cwt* command). The base wavelet chosen was the complex Morlet with a symmetry parameter (gamma) equal to 3 and a time-bandwidth product equal to 60. The wavelet coefficients were calculated at seventy logarithmic frequency points from 1 Hz to 125 Hz after which the squared absolute value of the coefficients resulted in a power scalogram.

All frequency power spectrums (Figure S6, S7) were obtained using FFT (Fast-Fourier Transform - MATLAB *fft* command). The FFT length chosen was the largest power of 2, less than the length of the observed iEEG trace. The coefficients were then normalized with the trace length. Finally, the squared absolute value of the spectral coefficients multiplied by 2 (one-sided FFT) resulted in the power spectrum.

Removing epileptiform activity—Data containing epileptiform activity was detected using a simplified version of methods from previous reports (Aghajan et al., 2017, Gelinas et al., 2016), using an envelope of 5 standard deviations above baseline raw iEEG activity. This procedure was applied after the *Mark* artifacts (used for synchronization) had been removed from the data and alignment of data streams had been completed. This resulted in an average of 1.27% of the data being removed across participants, similar to previous reports (Aghajan et al., 2017). While this method uses a simple thresholding approach, more sophisticated algorithms are available and can be used to improve detection accuracy in future studies (Gelinas et al., 2016; Staresina et al., 2015).

Removal of telemetry dropouts—Telemetry dropouts were manually detected and labeled during the experiments. The presence of dropouts was verified in post-analysis using the same method as for removing epileptiform activity once the synchronization had been completed.

Mo-DBRS command artifact detection—See the Mo-DBRS Synchronization section (Method Details).

Artifact rejection—See the Scalp EEG Artifact Reduction – Offline Processing section (Method Details).

Supplementary Material

Refer to Web version on PubMed Central for supplementary material.

ACKNOWLEDGMENTS

We thank Nader Shaterian and FabLab (Golden Beach, FL), Interactive Lab (Moscow, Russia), Merit Vick (NeuroPace, Inc.), and Jason Travis (NeuroPace, Inc.) for technical assistance. This work was supported by the National Institute of Neurological Disorders and Stroke (NS103802; NS058280), the McKnight Foundation (Technological Innovations in Neuroscience Award to N.S.), and the W.M. Keck Foundation (UCLA DGSOM Junior Faculty Award to N.S.). We also thank the participants for taking part in our study.

REFERENCES

Aghajan ZM, Villaroman D, Hiller S, Wishard TJ, Topalovic U, Christov-Moore L, Shaterian N, Hasulak NR, Knowlton B, Eliashiv D, Rao V, Fried I, Suthana N (2019). Modulation of human intracranial theta oscillations during freely moving spatial navigation and memory. BioRxiv. 738807. 10.1101/738807.

Aghajan ZM, Schuette P, Fields TA, Tran ME, Siddiqui SM, Hasulak NR, Tcheng TK, Eliashiv D, Mankin EA, Stern J, Fried I, and Suthana N (2017) Theta Oscillations in the Human Medial Temporal Lobe during Real-World Ambulatory. Curr. Biol. 27, 3743–3751.e3. [PubMed: 29199073]

Ant neuro, eego mylab, amplifier specifications. Available at: https://www.ant-neuro.com/products/eego_mylab/specs (Accessed: 01/04/2018).

Ant neuro, eego mylab, xensor. Available at: https://www.ant-neuro.com/products/xensor (Accessed: 07/05/2018).

Baud MO, Kleen JK, Mirro EA, Andrechak JC, King-Stephens D, Chang EF, Rao VR (2018). Multiday rhythms modulate seizure risk in epilepsy. Nat. Commun. 9, 1–10. [PubMed: 29317637]

Benabid AL, Pollak P, Louveau A, Henry S, de Rougemont J (1987). Combined (thalamotomy and stimulation) stereotactic surgery of the VIM thalamic nucleus for bilateral Parkinson disease. J. Appl. Neurophysiol. 50, 344–346.

Bohil CJ, Alicea B, Biocca FA (2011). Virtual reality in neuroscience research and therapy. Nat. Rev. Neurosci. 12, 752–762. [PubMed: 22048061]

Byrom B, McCarthy M, Schueler P, Muehlhausen W (2018). Brain Monitoring Devices in Neuroscience Clinical Research: The Potential of Remote Monitoring Using Sensors, Wearables, and Mobile Devices. Clin. Pharmacol. Ther. 104, 59–71. [PubMed: 29574776]

Gelinas JN, Khodagholy D, Thesen T, Devinsky O, Buzsáki G (2016). Interictal epileptiform discharges induce hippocampal-cortical coupling in temporal lobe epilepsy. Nat. Med. 22, 641–648. [PubMed: 27111281]

Gilron R, Little S, Perrone R, Wilt R, Hemptinne C. De, Yaroshinsky MS, Racine CA, Wang S, Ostrem JL, et al. (2020). Chronic wireless streaming of invasive neural recordings at home for circuit discovery and adaptive stimulation. BioRxiv. 10.1101/2020.02.13.948349.

Henin S, Shankar A, Hasulak N, Friedman D, Dugan P, Melloni L, Flinker A, Sarac C, Fang M, Doyle W, Tcheng T, Devinsky O, Davachi L, Liu A (2019). Hippocampal gamma predicts associative memory performance as measured by acute and chronic intracranial EEG. Sci. Rep 9, 593. [PubMed: 30679734]

Islam MK, Rastegarnia A, Yang Z (2016). Methods for artifact detection and removal from scalp EEG: A review. Clin. Neurophysiol. 46, 287–305.

Kassner M, Patera W, Bulling A (2014). Pupil. Proceedings of the 2014 ACM International Joint Conference on Pervasive and Ubiquitous Computing Adjunct Publication - UbiComp ‘14 Adjunct. 1151–1160.

Kremen V, Brinkmann BH, Kim I, Guragain H, Nasseri M, Magee AL, Attia T. Pal, Nejedly P, Sladky V, Chang S-Y, et al. (2018). Integrating brain implants with local and distributed computing devices: A next generation epilepsy management system. IEEE J. Transl. Eng. Health Med. 6, 2500112.

Ladouce S, Donaldson DI, Dudchenko PA, Ietswaart M (2017). Understanding minds in real-world environments: Toward a mobile cognition approach. Front. Hum. Neurosci. 10, 694. [PubMed: 28127283]

Lau-Zhu A, Lau MPH, McLoughlin G (2019). Mobile EEG in research on neurodevelopmental disorders: Opportunities and challenges. Dev. Cogn. Neurosci. 36, 100635.

Lozano AM, Fosdick L, Chakravarty MM, Leoutsakos JM, Munro C, Oh E, Drake KE, Lyman CH, Rosenberg PB, Anderson WS, Tang-Wai DF, et al. (2016). A Phase II Study of Fornix Deep Brain Stimulation in Mild Alzheimer's Disease. J. Alzheimers Dis. 54, 777–787. [PubMed: 27567810]

Meisenhelter S, Testorf ME, Gorenstein MA, Hasulak NR, Tcheng TK, Aronson JP, Jobst BC (2019). Cognitive tasks and human ambulatory electrocorticography using the RNS System. J. Neurosci. Methods. 311, 408–417. [PubMed: 30267724]

Nuttin B, Cosyns P, Demeulemeester H, Gybels J, Meyerson B (1999). Electrical stimulation in anterior limbs of internal capsules in patients with obsessive-compulsive disorder, Lancet 354, 1526.

O'Shea DJ, and Shenoy KV (2018). ERAASR: an algorithm for removing electrical stimulation artifacts from multielectrode array recordings. J. Neural Eng. 15, 026020.

Parvizi J, and Kastner S (2018). Promises and limitations of human intracranial electroencephalography. Nat. Neurosci. 21, 474–483. [PubMed: 29507407]

Ramantani G, Maillard L, Koessler L (2016). Correlation of invasive EEG and scalp EEG. Seizure 41, 196–200. [PubMed: 27324839]

Rao VR, Leonard MK, Kleen JK, Lucas BA, Mirro EA, Chang EF (2017). Chronic ambulatory electrocorticography from human speech cortex. NeuroImage 153, 273–282. [PubMed: 28396294]

Raspberry Pi Online Documentation. Available at: https://www.raspberrypi.org/documentation (Accessed: 10/01/2017).

Responsive Neurostimulator for Post-Traumatic Stress Disorder. Available at: https://clinicaltrials.gov/ct2/show/NCT04152993. Identifier: NCT04152993. (Accessed: 01/07/2020).

Ressler KJ, and Mayberg HS (2007). Targeting abnormal neural circuits in mood and anxiety disorders: from the laboratory to the clinic. Nat. Neurosci. 10, 1116–1124. [PubMed: 17726478]

Schulze-Bonhage A (2017). Brain stimulation as a neuromodulatory epilepsy therapy. Seizure 44, 169–175. [PubMed: 27876408]

Stanslaski S, Herron J, Chouinard T, Bourget D, Isaacson B, Kremen V, Opri E, Drew W, Brinkmann BH, Gunduz A, Adamski T, Worrell GA, Denison T (2018). A Chronically Implantable Neural Coprocessor for Investigating the Treatment of Neurological Disorders. IEEE Trans. Biomed. Circuits Syst. 12, 1230–1245. [PubMed: 30418885]

Staresina BP, Bergmann TO, Bonnefond M, Van Der Meij R, Jensen O, Deuker L, Elger CE, Axmacher N, Fell J (2015). Hierarchical nesting of slow oscillations, spindles and ripples in the human hippocampus during sleep. Nat. Neurosci. 18, 1679–1686. [PubMed: 26389842]

State-dependent Pathophysiological Oscillations in Parkinson's Disease and Treatment With DBS Using the Medtronic RC+S. Available at: https://clinicaltrials.gov/ct2/show/NCT04011449. Identifier: NCT04011449. (Accessed: 01/07/2020).

Suthana NA, Parikshak NN, Ekstrom AD, Ison MJ, Knowlton BJ, Bookheimer SY, Fried I (2015). Specific responses of human hippocampal neurons are associated with better memory. Proc. Natl. Acad. Sci. U.S.A. 112, 10503–10508. [PubMed: 26240357]

Suthana N, Aghajan ZM, Mankin EA, Lin A (2018). Reporting Guidelines and Issues to Consider for Using Intracranial Brain Stimulation in Studies of Human Declarative Memory. Front. Neurosci. 12, 905. [PubMed: 30564089]

Suthana N, Haneef Z, Stern J, Mukamel R, Behnke E, Knowlton B, Fried I (2012). Memory enhancement and deep-brain stimulation of the entorhinal area. N. Engl. J. Med. 366, 502–510. [PubMed: 22316444]

The Motor Network in Parkinson's Disease and Dystonia: Mechanisms of Therapy. Available at: https://clinicaltrials.gov/ct2/show/NCT03582891. Identifier: NCT03582891. (Accessed: 01/07/2020).

Vidailhet M, Vercueil L, Houeto JL, Krystkowiak P, Benabid AL, Cornu P, Lagrange C, Montcel S. T. du, Dormont D, Grand S, et al. (2005). Bilateral deep-brain stimulation of the globus pallidus in primary generalized dystonia. N. Engl. J. Med. 352, 459–467. [PubMed: 15689584]

Wu H, Miller KJ, Blumenfeld Z, Williams NR, Ravikumar VK, Lee KE, Kakusa B, Sacchet MD, Wintermark M, Christoffel DJ, Rutt BK, Bronte-Stewart H, Knutson B, Malenka RC, Halpern CH (2018). Closing the loop on impulsivity via nucleus accumbens delta-band activity in mice and man. Proc. Natl. Acad. Sci. U.S.A. 115, 192–197. [PubMed: 29255043]

Zaitsev M, Maclaren J, and Herbst M (2015). Motion artifacts in MRI: A complex problem with many partial solutions. J. Magn. Reson. Imaging 42, 887–901. [PubMed: 25630632]

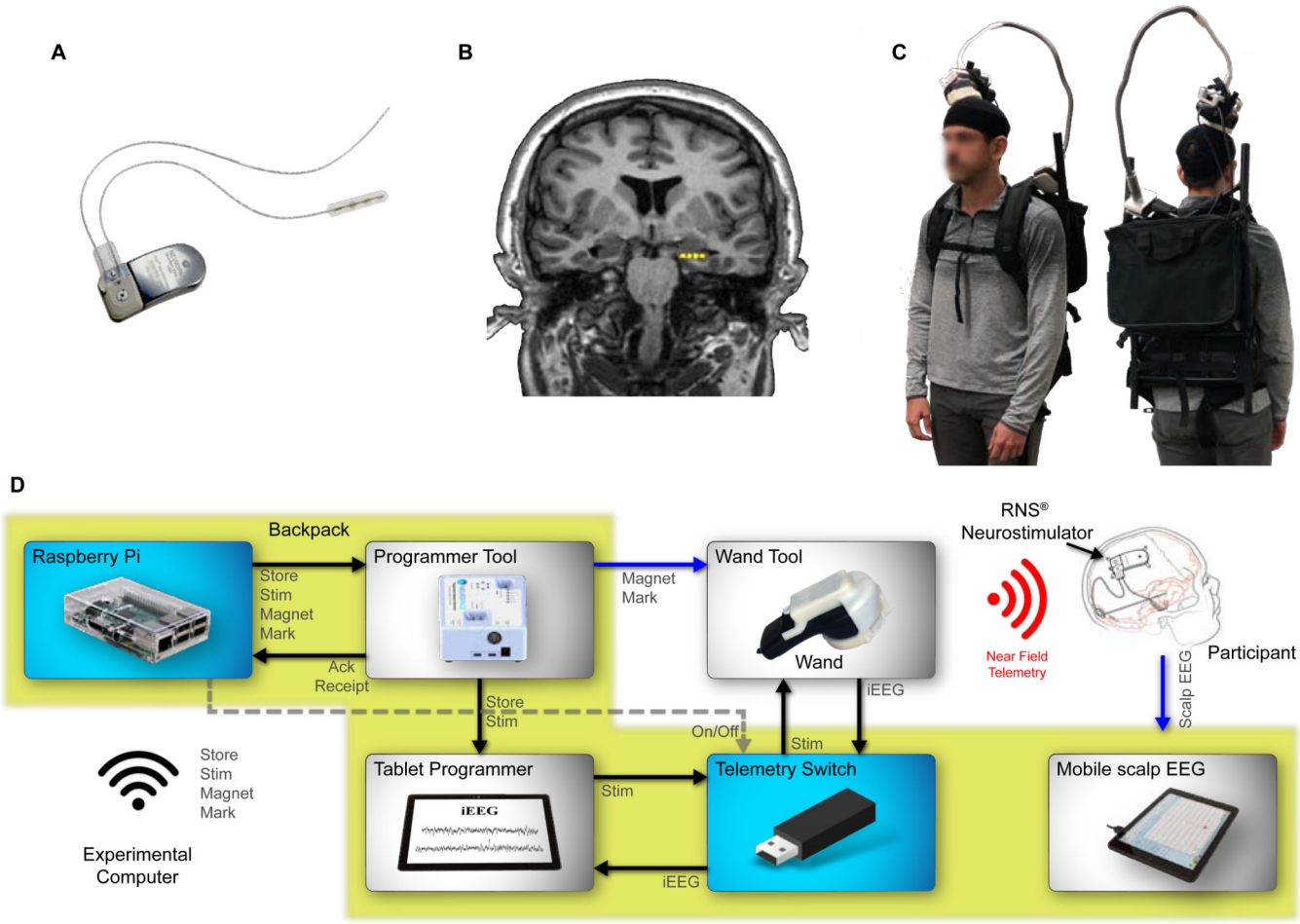

Figure 1. Mobile Deep Brain Recording and Stimulation (Mo-DBRS) platform

(A) The RNS Neurostimulator model RNS-300M with two leads containing eight electrode contacts.

(B) A participant's magnetic resonance imaging (MRI) scan showing four-electrode contact locations (yellow) in the left hippocampus (electrode locations determined by co-registering a post-implant computerized tomography (CT) scan.

(C) Mo-DBRS Full version with a wearable backpack that carries the Research Tools.

(D) Mo-DBRS Research Tools receive commands (*Store*, *Stim*, *Magnet*, *Mark*) from an Experimental Computer. A Raspberry Pi (RP) serves as an input to the Research Tools, via wireless forwarding of commands to the Programmer Tool which are then implemented in the Programmer (Tablet or Laptop) or Wand Tool. The Wand (black), which sends data to and from the implanted RNS Neurostimulator, is enclosed in the Wand Tool (white), which executes *Magnet* and *Mark* commands. The Wand wirelessly transmits the commands from the Programmer (*Store* and *Stim*) to the implanted RNS Neurostimulator. Yellow highlighted items are Research Tools that can be carried in a backpack. Shown is the Tablet Programmer; however, the same setup applies if using the Laptop Programmer (discontinued by NeuroPace). Solid black arrows indicate a USB serial connection. Solid blue arrows indicate a custom, proprietary connection. Dashed arrows indicate a single wired connection. Black and red Wi-Fi symbols indicate a wireless local network connection and Near Field

Telemetry, respectively. The Telemetry Switch is a USB device serving as a bridge between the Programmer and the Wand that can turn telemetry on/off and is controlled by RP.

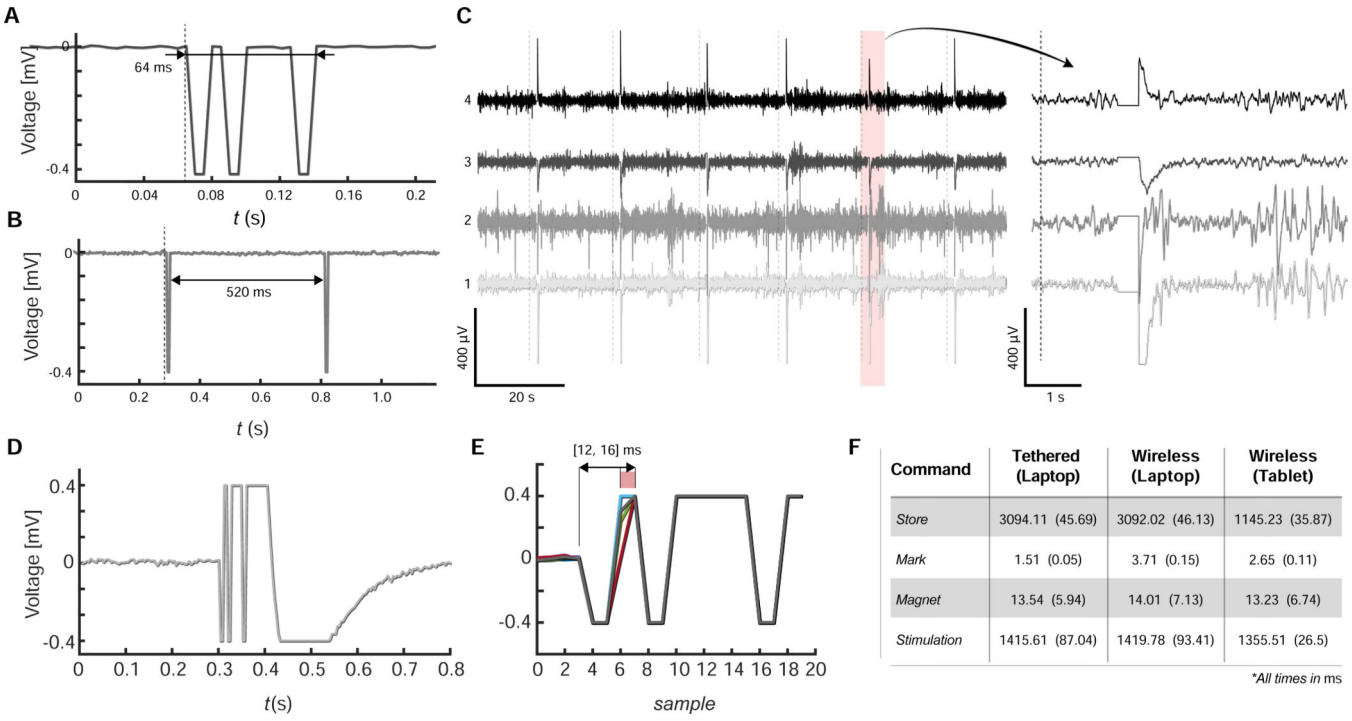

F

Command	Tethered (Laptop)	Wireless (Laptop)	Wireless (Tablet)
Store	3094.11 (45.69)	3092.02 (46.13)	1145.23 (35.87)
Mark	1.51 (0.05)	3.71 (0.15)	2.65 (0.11)
Magnet	13.54 (5.94)	14.01 (7.13)	13.23 (6.74)
Stimulation	1415.61 (87.04)	1419.78 (93.41)	1355.51 (26.5)

**All times in* ms

Figure 2. Characterization of Mo-DBRS command latencies

(A) In-vivo Real-Time iEEG data during a remotely delivered *Mark* command tested in-vivo. A single *Mark* signal has a distinctive pattern with 3 spikes, 16 sample points long (64 ms), and can be easily detected in post-processing procedures for synchronization purposes.

(B) An iEEG artifact (duration 520 ms) resulting from a remotely delivered *Magnet* signal recorded in Real-Time iEEG data in-vivo. Shown is the full electromagnetic pulse (520 ms duration).

(C) In-vivo Real-Time iEEG activity showing 6 remotely delivered iES bursts (via the *Stim* command) with a 20 s inter-stimulation interval.

(D) Ex-vivo testing showing a Real-Time iEEG captured *Mark* signal and a simultaneous Reference Pulse sent to the same iEEG channel being recorded.

(E) Zoomed-in view of Real-Time iEEG (from D), showing that the *Mark* signal arrives before the Reference Pulse. In 10 test trials (different line colors), the offset (relative latency) was 12–16 ms between the *Mark* command and Reference Pulse. Given the sampling period of 4 ms, this reflects the synchronization accuracy that can be achieved using the *Mark* command.

(F) Summarized absolute latencies for each command (*Store*, *Mark*, *Magnet*, and *Stim*) from the Raspberry Pi (RP) during tethered and wireless setups with the Laptop or Tablet Programmer. Note that absolute latencies for the *Store* command were measured with respect to the end of command delivery while for *Stim, Mark*, and *Magnet* they were measured with respect to the onset of the associated signal in the iEEG.

Dotted lines represent command initiation.

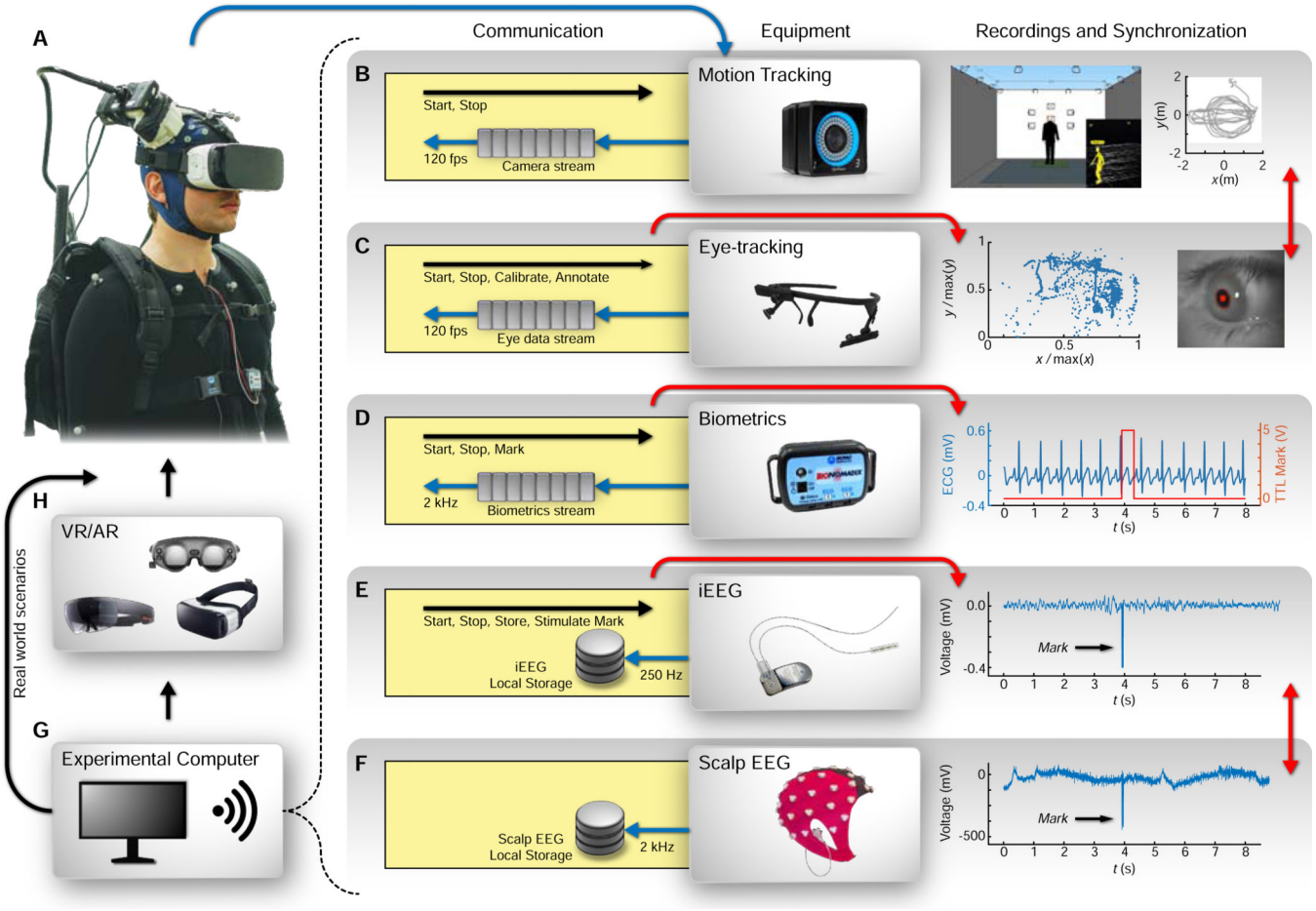

Figure 3. Wearable technologies included in the Mo-DBRS platform

Wearables listed (B–F), including their wireless connection with the Experimental Computer, a synchronization solution, and an example data trace for each. Yellow boxes reflect the communication flow between the Experimental Computer and wearables. Black arrows show the communication flow (commands sent). Blue arrows show the data flow (gray boxes indicate real-time data transfer and gray circles indicate on-device storage). Red arrows point to one possible synchronization solution.

(A) A participant wearing the full Mo-DBRS platform with a VR headset.

(B) Wall-mounted cameras for 3-D full-body motion capture used to record real-time position and movement streaming at a rate of 120 fps. Cameras are connected through the local wireless network, and a pre-configured recording is controlled with a start/stop function. Recording box shows an example real-time view of the participant's location (left) and an extracted top-down view of the participant's movement (right).

(C) A wearable eye-tracking system with 120 fps head direction camera and 200 fps eye cameras. Eye-tracking is synchronized with wearable or wall-mounted motion capture (B) cameras, or with LEDs/annotations triggered from within the Experimental Task Paradigm controlled via the Experimental Computer. The eye-tracking headset is connected through the local wireless network awaiting *Start, Stop, Calibrate,* or *Annotate* commands. The

recording box shows a snapshot view from one eye-tracking camera (right) and a 2D projection of pupil movement (left).

(D) Wearable biometric system for heart rate, skin conductance, and respiration measurements. The recording box shows an ECG recording trace in line with a signal containing a 400 ms wide synchronization pulse.

(E) The wireless implantable RNS Neurostimulator is connected/synchronized with the Experimental Task Paradigm controlled by the Experimental Computer through the local wireless network via the RP. The recording box shows example raw Real-Time iEEG data with an example *Mark* command signal used for synchronization.

(F) Wearable scalp EEG cap. The recording box shows an example scalp EEG data trace with an example *Mark* command signal used for synchronization.

(G) Experimental Computer (e.g., laptop, tablet, or phone) running the Experimental Task Paradigm.

(H) Example integrated VR/AR headsets are shown, including the SMI modified Samsung Gear VR, Microsoft HoloLens, and Magic Leap. In this case the Experimental Computer runs on the VR/AR headset. For studies done in a real-world environment, an eye-tracking headset shown in (C**)** can be used instead.

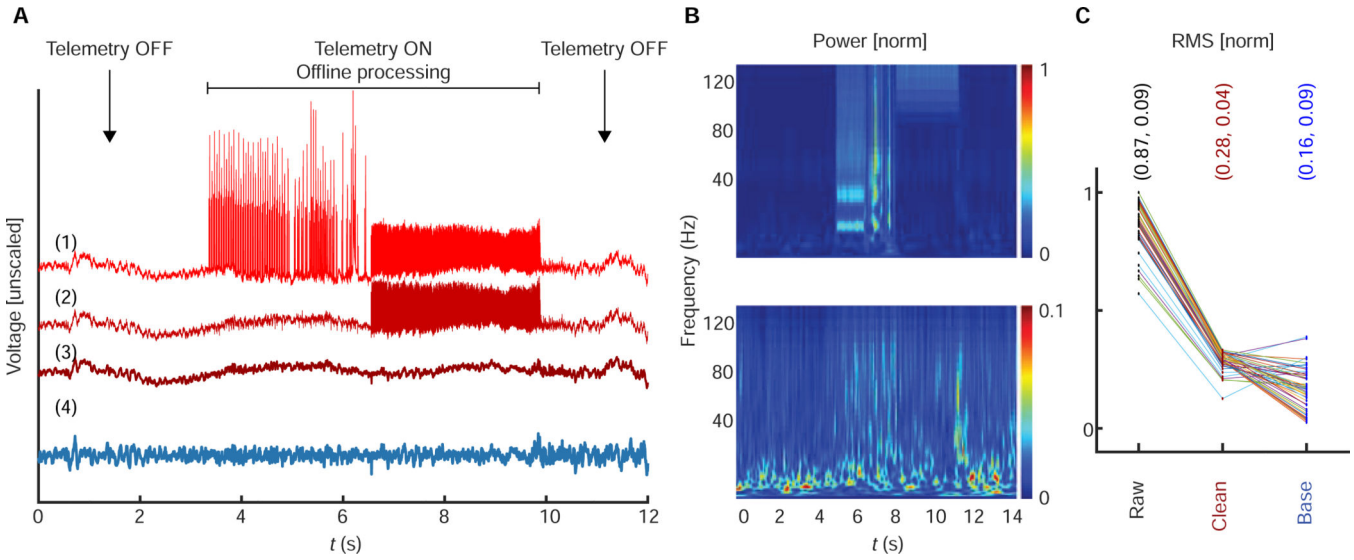

Figure 4. Artifact rejection solution for simultaneous iEEG and scalp EEG

Steps used for artifact reduction shown in an example scalp EEG channel:

(A) Results of using the Telemetry Switch (Telemetry ON/OFF) and offline processing (steps 1–4, see STAR Methods).

(B) Time-frequency power scaleogram of raw (top) and cleaned (bottom) scalp EEG.

(C) Normalized RMS value (mean, s.d.) of the signal for all channels before and after cleaning, as well as comparison with RMS of the corresponding baseline scalp EEG, unaffected by artifacts.

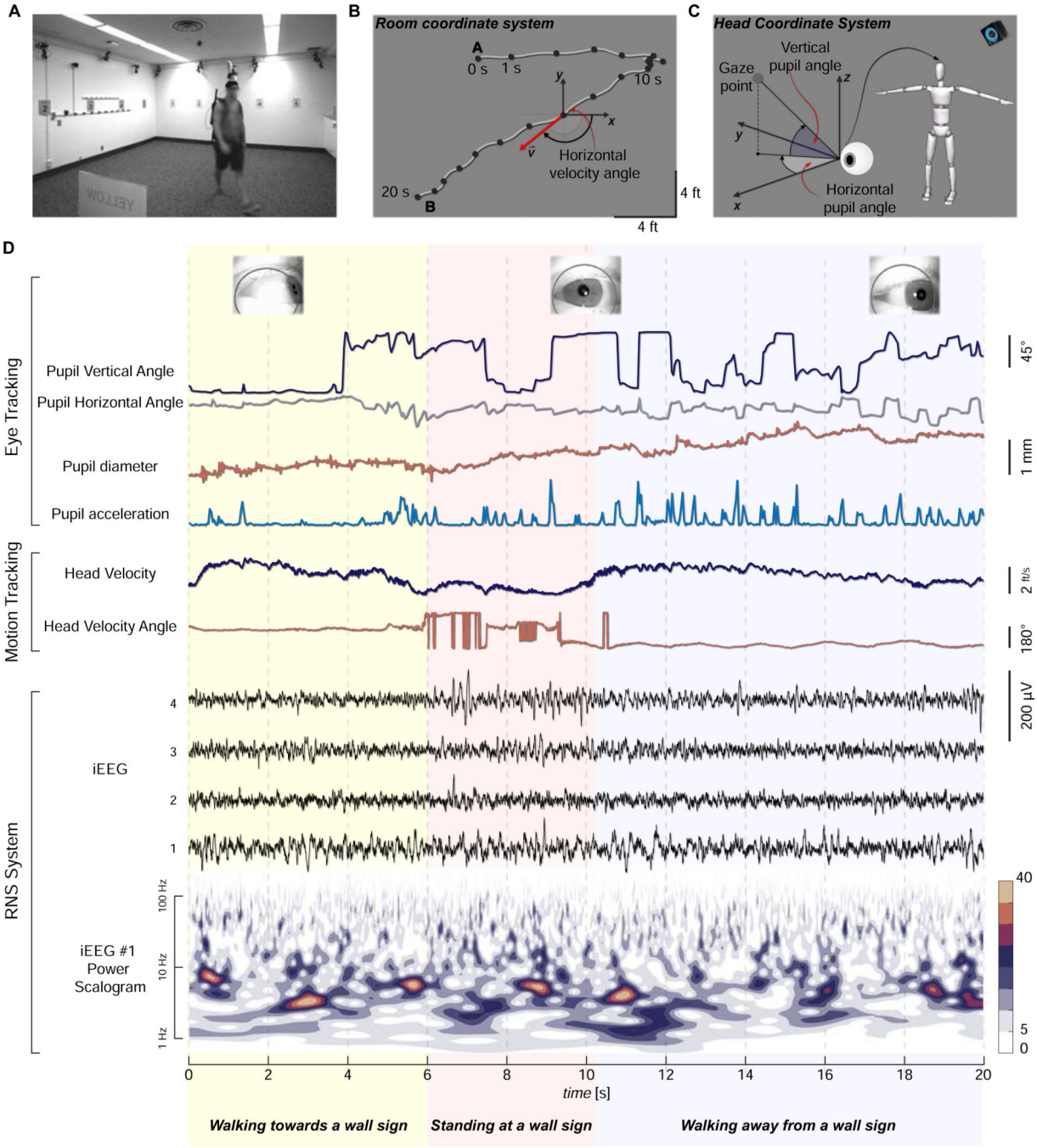

Figure 5. Simultaneous measurements of neural activity and other behavioral variables in a freely moving human

(A) A photo, taken using a wall-mounted camera, of a participant completing a spatial navigation task.

(B) Top-down view of the room with an example participant's trajectory during a 20-second walk (from point A to B) extracted from Motion Capture data. Black dots from A to B along the path represent where the participant is after 1, 2, …, 20 s. Also shown is a room coordinate system and the defined velocity vector. Z-axis is not shown for simplicity.

(C) Eye movements were tracked using a head coordinate system (in which horizontal and vertical angles are defined). To obtain absolute eye movements with respect to the room coordinate system, head movements were extracted from the Motion Capture data and then used to convert eye movements from the head to the room coordinate system in three dimensions.

(D) Raw and synchronized iEEG from 4 bipolar recording channels, motion capture, and eye-tracking data is shown from the same participant, captured during the 20-second walking period. Position of the participant's pupils at 3 time points is highlighted in different background colors. Body and eye motion variables correspond to the vectors defined in (B) and (C).

Figure 6. Additional photos of the Mo-DBRS platform in naturalistic and laboratory settings

(A) A participant wearing the Mo-DBRS Full platform showing the backpack connected to the Wand.

(B) A participant performing a laboratory-based stationary task.

(C) Wearable equipment for biometric recordings, including a respiration belt, skin conductance and heart rate sensor.

(D) A participant wearing the Mo-DBRS Full platform with the Magic Leap AR headset in a laboratory equipped with wall-mounted motion capture cameras.

Table 1.

Comparison of Mo-DBRS with previous studies that used the RNS System

Three key features are compared, including capability for use during ambulatory behaviors (Mobility), integration with wearable technologies (Wearables), synchronization method (Sync method), relative latency (mean) of iEEG synchronization with the Experimental Task Paradigm (Task-iEEG Sync relative latency (mean)), and relative latency (s.d.) of iEEG synchronization with the Experimental Task Paradigm (Task-iEEG Sync relative latency (s.d.)). NR refers to not reported.

	Mo-DBRS Full	**Mo-DBRS Lite**	**Meisenhelter et al.**	**Aghajan et al.**	**Rao et al.**	**Rao et al.**
Mobility	Yes	Yes	No	Yes	No	Yes
Wearables	Yes	Yes	No	No	No	No
Sync method	*Mark*	*Magnet*+LED	*Mark*	*Magnet*+LED	Video	Neural Response
Task-iEEG Sync relative latency (mean)	14 ms	432 ms	NR	NR	NR	NR
Task-iEEG Sync relative latency (s.d.)	2 ms	83 ms	4 ms	125 ms	60 ms	30 ms

Table 2.

Mo-DBRS Full versus Lite

Mo-DBRS setup options and whether they allow for Real-Time iEEG, Magnet-triggered iEEG (Magnet iEEG), or iES. Methods for synchronization of iEEG with the Experimental Task Program (iEEG-task sync) and scalp EEG (iEEG-scalp EEG sync), and the associated relative latencies and solutions for minimizing telemetry-related artifacts are also shown. Presented relative latencies (mean ± s.d.) are rounded.

Setup Options	Real-Time View	iES Control	Task - iEEG Sync	Relative Latency (ms)	Scalp EEG - iEEG Sync	Relative Latency (ms)	Telemetry artifact solution for scalp EEG	Wearabiility	Weight (lbs)
Mo-DBRS Full Real-Time iEEG	Yes	Yes	*Mark*	14 ± 2	*Mark*	16 ± 4	Offline processing	Full wearable platform	~ 9
Mo-DBRS Lite Magnet iEEG	No	No	*LED / Magnet*	432 ± 83/ 424 ± 79	*Magnet*	424 ± 79	None	Lightweight wearable platform	~ 1
Mo-DBRS Full Real-Time + Magnet iEEG	Yes	Yes	*Mark / Magnet*	14 ± 2/424 ± 79	*Mark / Magnet / Stim*	16 ± 4/426 ± 81/2 ± 2	Telemetry switch + Offline processing	Full wearable platform	~ 9

KEY RESOURCES TABLE

REAGENT or RESOURCE	SOURCE	IDENTIFIER
Software and Algorithms		
MATLAB R2018A	The MathWorks	https://www.mathworks.com/products/matlab/
Python 2.7	Python Software Foundation	https://www.python.org/download/releases/2.7/
Unity 2018.4.14f1	Unity Technologies	https://unity3d.com/get-unity/download/archive/
Mo-DBRS Custom Scripts	This work	https://github.com/suthanalab/Mo-DBRS
Other		
Raspberry Pi 3 Model B+	Raspberry Pi Foundation	https://www.raspberrypi.org/products/raspberry-pi-3-model-b-plus/
Pupil Labs Core	Pupil Labs	https://pupil-labs.com/products/core/
Optitrack Motion Capture	Natural Point, Inc	https://optitrack.com/products/primex-13/
Mobile Scalp EEG	ANT Neuro	https://www.ant-neuro.com/products/eego_mylab
Biometric Measurements	Biopac Systems, Inc	https://www.biopac.com/research/
Mo-DBRS Custom Hardware	This work	https://github.com/suthanalab/Mo-DBRS